Complexes Derived from the Reaction of Manganese(III) Schiff Base Complexes and Hexacyanoferrate(III): Syntheses, Multidimensional Network Structures, and Magnetic Properties

Hitoshi Miyasaka,[†] Naohide Matsumoto,*[,†] Hisashi Ōkawa,[†] Nazzareno Re,[‡] Emma Gallo,[§] and Carlo Floriani*[,§]

Contribution from the Department of Chemistry, Faculty of Science, Kyushu University, Hakozaki, Higashi-ku, Fukuoka 812, Japan, Dipartimento di Chimica, Università di Perugia, I-06100 Perugia, Italy, and Institut de Chimie Minérale et Analytique, BCH, Université de Lausanne, CH-1015 Lausanne, Switzerland

Received August 9, 1995[⊗]

Abstract: The reaction between the $[Mn(BS)(H_2O)]^+$ monomeric and $[Mn_2(\mu\text{-}BS)_2(H_2O)_2]^{2+}$ dimeric cations and $[Fe(CN)_6]^{3-}$ gave rise to cation−anion interaction *via* the formation of [Fe−C≡N−Mn] bridges. Depending on the nature of the Schiff base and regardless of the stoichiometry used, either the trimeric anion $[\{Mn(BS)\}_2\{Fe(CN)_6\}]^-$ (BS = 3-MeOsalen, **6**; 5-Clsalen, **7**; 5-Brsalen, **8**; salcy, **10**) or the pentameric cation $[\{Mn(BS)\}_4\{Fe(CN)_6\}]^+$ (BS = saltmen, **9**) is formed, which has been assembled by the K^+ cation or the ClO_4^- anion, respectively. The X-ray analysis of **6** revealed a two-dimensional network layer structure. The magnetic measurements showed its metamagnetic behavior, where the ferromagnetic interaction operates within each layer and the antiferromagnetic interaction operates between the layers. The Neel temperature, T_N, is 9.2 K, and the critical field at 2 K is 300 Oe. The temperature dependent magnetic susceptibilities of **7** and **8** are in agreement with a discrete, symmetrical, trinuclear structure Mn(III)−Fe(III)−Mn(III) ($S_{Mn} = 2$, $S_{Fe} = 1/2$, $S_{Mn} = 2$) with a ferromagnetic spin coupling between the Mn(III) and Fe(III) ions, a small antiferromagnetic intertrimer interaction, and a large zero-field splitting of the Mn(III) ion. The structure of **9** consists of a two-dimensional layer containing as the repeating unit a cyclic dodecamer. The layers stack along the *c* axis, and ClO_4^- anions are positioned between the layers. The magnetic measurements showed this compound's ferromagnetic behavior. There are, in fact, two kinds of intralayer magnetic interactions, the interaction between the Fe(III) and Mn(III) ions bridged by CN groups and the interaction between two Mn(III) ions in the dimer $[Mn_2(saltmen)_2]$, both being ferromagnetic. The interlayer magnetic interaction is ferromagnetic. All of the interactions render to **9** an overall ferromagnetic behavior.

Introduction

The field of molecular magnetism has undergone quite spectacular advances in the last decade.[1] Several different approaches are currently used in order to design and synthesize molecular-based magnetic materials exhibiting spontaneous magnetization. The discovery of the first pure organic ferromagnet in the *β*-crystalline form of *p*-nitrophenyl nitronyl nitroxide in 1991 by Kinoshita and co-workers[2] has inspired studies on the structure and magnetism of organic radicals.[3] On the other hand, ferromagnetic and ferrimagnetic one-dimensional chain compounds based upon metal complexes have achieved noteworthy success in the area of molecular design, synthesis, magnetism, and theoretical studies:[1,4] the organic−organometallic, charge-transfer complex $[Fe(Me_5Cp)_2]^+[TCNE]^-$ (Me_5-Cp = pentamethylcyclopentadienyl and $TCNE^-$ = tetracyanoethylene anion radical) by Miller and Epstein,[5] the inorganic−inorganic, oxalato-bridged Mn(II)−Cu(II) complex $\{MnCu(pbaOH)(H_2O)_3\}_n$ ($pbaOH^{4-}$ = 2-hydroxy-1,3-propylenebis(oxamato) anion) by Kahn and co-workers,[6] and the inorganic−organic, Mn(II)−radical complex $\{Mn(hfac)_2(NITR)\}_n$ ($hfac^-$ = (hexafluoroacetyl)acetonato anion and NITR = 2(*R*)-4,4,5,5-tetramethyl-4,5-dihydro-1*H*-imidazolyl-1-oxy 3-oxide, R = Et, Pr^n, Pr^i) by Gatteschi and co-workers.[7] However, although it

[†] Kyushu University.
[‡] Università di Perugia.
[§] Université de Lausanne.
[⊗] Abstract published in *Advance ACS Abstracts,* January 15, 1996.

(1) (a) Kahn, O. *Molecular Magnetism*; VCH: Weinheim, Germany, 1993. (b) *Magnetic Molecular Materials*; Gatteschi, D., Kahn, O., Miller, J. S., Palacio, F., Eds.; NATO ASI Series E; Kluwer Academic: Dordrecht, The Netherlands, 1991; Vol. 198. (c) Iwamura, H.; Miller, J. S. Proceedings of the Symposium on the Chemistry and Physics of Molecular Based Magnetic Materials. *Mol. Cryst. Liq. Cryst.* **1993**, 232−233. (d) Miller, J. S.; Epstein, A. J. *Angew. Chem., Int. Ed. Engl.* **1994**, *33*, 399. (e) Miller, J. S.; Epstein A. J. *Angew. Chem., Int. Ed. Engl.* **1994**, *33*, 385. (f) Caneschi, A.; Gatteschi, D.; Sessoli, R.; Rey, P. *Acc. Chem. Res.* **1989**, *22*, 392. (g) Caneschi, A.; Gatteschi, D.; Rey, P. *Prog. Inorg. Chem.* **1989**, *22*, 392.

(2) (a) Le, L. P.; Keren, A.; Luke, G. M.; Wu, W. D.; Uemura, Y. J.; Tamura, M.; Ishikawa, M.; Kinoshita, M. *Chem. Phys. Lett.* **1993**, *206*, 405. (b) Kinoshita, M. *Synth. Met.* **1993**, *56*, 3285.

(3) (a) Kinoshita, M. *Mol. Cryst. Liq. Cryst.* **1993**, *232*, 1. (b) Kinoshita, M. *Mol. Cryst. Liq. Cryst.* **1989**, *176*, 163. (c) Awaga, K.; Sugano, T.; Kinoshita, M. *Chem. Phys. Lett.* **1987**, *141*, 540. (d) Tamura, M.; Nakazawa, Y.; Shiomi, D.; Nazawa, K.; Hosokoshi, Y.; Ishikawa, M.; Takahashi, M.; and Kinoshita, M. *Chem. Phys. Lett.* **1991**, *186*, 401. (e) Chiarelli, R.; Rassat, A.; Rey, P. *J. Chem. Soc., Chem. Commun.* **1992**, 1081. (f) Chiarelli, R.; Navak, M. A.; Rassat, A.; Tholence, J. L. *Nature* **1993**, *363*, 147. (g) Nagami, T.; Tomioka, K.; Ishida, T.; Yoshikawa, H.; Yasui, M.; Iwasaka, F.; Iwamura, H.; Takeda, N.; Ishikawa, M. *Chem. Lett.* **1994**, 29. (h) Ishida, T.; Tsuboi, H.; Nagami, T.; Yoshikawa, H.; Yasui, M.; Iwasaka, F.; Iwamura, H.; Takeda, N.; Ishikawa, M. *Chem. Lett.* **1994**, 919. (j) Yee, G. T.; Manriquez, J. M.; Dixon, D. A.; McLean, R. S.; Groski, D, M.; Flippen, R. B.; Narayan, K. S.; Epstein, A. J.; Miller, J. S. *Adv. Mater.* **1991**, *3*, 309. (k) Broderick, W. E.; Thompson, J. A.; Day, E. P.; Hoffman, B. M. *Science* **1990**, *249*, 401. (l) Broderick, J. A.; Hoffman, B. M. *J. Am. Chem. Soc.* **1991**, *113*, 6334. (m) Miller, J. S.; Calabrese, J. C.; McLean, R. S.; Epstein, A. J. *Adv. Mater.* **1992**, *4*, 498.

(4) (a) Kahn, O. *Structure and Bonding*; Springer: Berlin, Heidelberg, 1987, Vol. 68. (b) Nakatani, K.; Carriat, J. Y.; Journaux, Y.; Kahn, O.; Lloret, F.; Renard, J. P.; Pei, Y.; Sletten, J.; Verdaguer, M. *J. Am. Chem. Soc.* **1989**, *111*, 5739. (c) Gleizes, A.; Verdaguer, M. *J. Am. Chem. Soc.* **1981**, *103*, 7373. (d) Gleizes, A.; Verdaguer, M. *J. Am. Chem. Soc.* **1984**, *106*, 3727.

(5) Miller, J. S.; Epstein, A. J.; Reiff, W. M. *Chem. Rev.* **1988**, *88*, 201.

(6) Kahn, O.; Pei, Y.; Verdaguer, M.; Renard, J. P.; Sletten, J. *J. Am. Chem. Soc.* **1998**, *110*, 782.

0002-7863/96/1518-0981$12.00/0

is easier to design strategies for one-dimensional compounds, recent efforts have been directed to the design of multidimensional magnetic compounds since ferromagnetism itself is a three-dimensional property. Along this line, mixed-metal and mixed-valence assemblies have attracted much attention.[1] Matsumoto et al. reported a series of metal-complex based ferromagnets $\{NBu_4[MCr(ox)_3]\}_x$ (M = Mn^{2+}, Fe^{2+}, Co^{2+}, Ni^{2+}, and Cu^{2+}) that are designed to form multidimensional network structures by assembling alternately the D_3-symmetric, η^3-complex $Cr(ox)_3^{3-}$ and the metal(II) ion.[8,9] Kahn et al. reported the crystal structure and spontaneous magnetization (T_c = 22.5 K) of a three-dimensional mixed-metal assembly, $(rad)_2Mn_2[Cu(opba)]_3(DMSO)_2\cdot 2H_2O$ (rad^+ = 2-(4-*N*-methylpyridinium)-4,4,5,5-tetramethylimidazoline-1-oxyl 3-oxide, opba = *o*-phenylenebis(oxamato)).[10] Babel et al.,[11] and later Verdaguer et al.,[12] have revealed that the cyanide system based on the Prussian blue family $CA^{II}[B^{III}(CN)_6]$ (A^{II} = divalent magnetic metal ion, B^{III} = trivalent magnetic metal ion, and C = monovalent nonmagnetic metal ion) exhibits an excellent molecular design which gives ferri- and ferromagnets, due to the three-dimensional alternate array of A^{II} and B^{III}. Among the cyanide complexes, a compound exhibiting a high magnetic-ordering temperature of T_c = 240 K was reported recently.[13] The inconvenience of this system arises from chemical difficulties in characterizing the materials, which precipitate with a variable number of water molecules, $CA[B(CN)_6]\cdot H_2O$, and which give single crystals with great difficulty. Since this type of compound is still very limited, it is desirable to develop a novel family of multidimensional magnetic compounds that make it possible to investigate the detailed correlation between the crystal structure and the magnetic property.

We report here extended structures derived from the reaction between the cationic complexes $[Mn(BS)(H_2O)]^+$ and $[Mn_2(BS)_2(H_2O)_2]^{2+}$ (BS = 3-MeOsalen = *N*,*N*′-ethylenebis(3-methoxysalicylideneiminato) dianion; 5-Clsalen = *N*,*N*′-ethylenebis(5-chlorosalicylideneiminato) dianion; 5-Brsalen = *N*,*N*′-ethylenebis(5-bromosalicylideneiminato) dianion; saltmen = *N*,*N*′-(1,1,2,2-tetramethylethylene)bis(salicylideneiminato) dianion; and salcy = *N*,*N*′-(*trans*-1,2-cyclohexanediylethylene)bis(salicylideneiminato) dianion) and the anion $[Fe(CN)_6]^{3-}$.

The Mn−Fe interaction is achieved via the bridging bonding mode of C≡N, while the polymetallic units are assembled by the intervention of cations K^+ and anions $(ClO_4)^-$.

Depending on the steric properties and the substituents of the quadridentate Schiff-base ligand around Mn, we identified two classes of extended structures. The first one derives from the assembly of a trimeric unit $[\{Mn(BS)\}_2\{Fe(CN)_6\}]^-$ by the K^+ cation, while in the second one the pentameric cation $[\{Mn(BS)\}_4\{Fe(CN)_6\}]^+$ is assembled by ClO_4^- anions. Since the X-ray analysis for representative compounds of both classes revealed two unique two-dimensional layer structures consisting of a cyclic octamer $[(-Mn-NC-Fe-CN-)]_4$ and a cyclic dodecamer $[(-NC-Fe-CN-Mn\cdots Mn)]_4$ as the net unit and their magnetic measurements including the temperature dependence of magnetic susceptibility, field dependence of magnetization up to 55 kOe under various temperatures, hysteresis loop, magnetization under zero and weak magnetic fields revealed the spontaneous magnetic ordering due to the metamagnetism and ferromagnetism, the crystal structures and the magnetic properties are reported. Some preliminary results have already been reported.[14]

Results and Discussion

The reaction between the two building blocks $[Mn(BS)(H_2O)]^+$ [BS = salen-substituted tetradentate Schiff base ligand] and $[Fe(CN)_6]^{3-}$ has been used for a complex−complex d^4-d^5 aggregation achieved thanks to the bridging bonding mode exhibited by the CN^- ligand in $[Fe(CN)_6]^{3-}$. The experimental procedure consists in mixing $[Mn(BS)(H_2O)]ClO_4$ and $K_3[Fe(CN)_6]$ in a methanol−water solution. The cationic manganese derivative can be present in solution mainly as a monomer **A** or as a dimer **B** depending on the steric characteristics of the

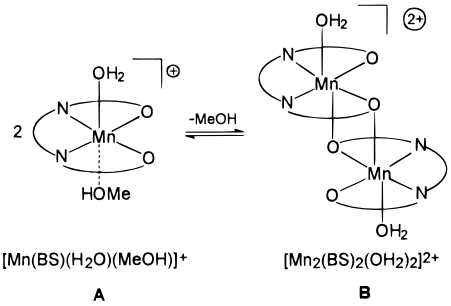

(1)

Schiff base. The interconversion between the two forms, depending on the reaction conditions, is a very probable process. Structural evidences for both cations have been obtained from the crystallization of $[Mn(salen)][(H_2O)(MeOH)]^+$ and $[Mn_2(salen)_2(H_2O)_2]^{2+}$ out of the same reaction (*vide infra*).

This equilibrium would affect the nature of the aggregate formed in the reaction with $[Fe(CN)_6]^{3-}$. Herein the cationic starting material, regardless of the possible form in solution, will be abbreviated as $[Mn(BS)(H_2O)]ClO_4$ [BS = MeOsalen, **1**; 5-Clsalen, **2**; 5-Brsalen, **3**; saltmen, **4**; salcy, **5**].

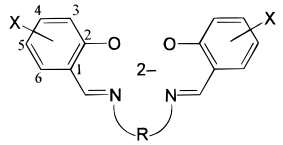

X = 3-MeO, R = en, **1**
X = 5-Cl, R = en, **2**
X = 5-Br, R = en, **3**
X = H, R = tmen, **4**
X = H, R = Cy, **5**

The reaction between $[Mn(BS)(H_2O)]ClO_4$ and $K_3[Fe(CN)_6]$ gave, regardless of the Mn:Fe molar ratio, different aggregates as a function of the Schiff base ligand only (see Schemes 1−4). Thus, the reaction was always carried out in a Mn:Fe = 1:1 molar ratio. Compounds from Schemes 1−4 have been obtained

(7) (a) Caneschi, A.; Gatteschi, D.; Renard, J. P.; Rey. P.; Sessoli, R. *Inorg. Chem.* **1989**, *28*, 1976. (b) Caneschi, A.; Gatteschi, D.; Renard, J. P.; Rey. P.; Sessoli, R. *Inorg. Chem.* **1989**, *28*, 3314. (c) Caneschi, A.; Gatteschi, D.; Rey. P.; Sessoli, R. *Inorg. Chem.* **1991**, *30*, 3937. (d) Benelli, C.; Caneschi, A.; Gatteschi, D.; Sessoli, R. *Inorg. Chem.* **1993**, *32*, 4797. (e) Caneschi, A.; Gatteschi, D.; Sessoli, R. *Inorg. Chem.* **1993**, *32*, 4612.

(8) (a) Tamaki, H.; Zhong, Z. J.; Matsumoto, N.; Kida, S.; Koikawa, M.; Achiwa, N.; Hashimoto, Y.; Ōkawa, H. *J. Am. Chem. Soc.* **1992**, *114*, 6974. (b) Zhong, Z. J.: Matsumoto, N.; Ōkawa, H.; Kida, S. *Chem. Lett.* **1990**, 87. (c) Tamaki, H.; Mitsumi, M.; Nakamura, K.; Matsumoto, N.; Kida, S.; Ōkawa, H.; Iijima, S. *Chem. Lett.* **1992**, 1975.

(9) Recently Decurtins et al. succeeded in obtaining a the single-crystal X-ray analysis of the analogue compound $\{[P(Ph)_4][MnCr(ox)_3]\}_n$ and revealed its two-dimensional layer structure. Decurtins, S.; Schmalle, H. W.; Oswald, H. R.; Linden, A.; Ensling, J.; Gütlich, P.; Hauser, A. *Inorg. Chim. Acta* **1994**, *216*, 65.

(10) Stumpf, H. O.; Ouahab, L.; Pei, Y.; Grandjean, D.; Kahn, O. *Science* **1993**, *261*, 447.

(11) Grieber, W. D.; Babel, D. *Z. Naturforsch.* **1982**, *87b*, 832.

(12) (a) Gadet, V.; Mallah, T.; Castro, I.; Veillet, P.; Verdaguer, M. *J. Am. Chem. Soc.* **1992**, *114*, 9213. (b) Ito, A.; Suenaga, M.; Ono, K.; *J. Chem. Phys.* **1968**, *48*, 3597.

(13) Mallah, T.; Thiebault, S. Verdaguer, M.; Veillet, P. *Science* **1993**, *262*, 1555.

(14) Miyasaka, H.; Matsumoto, N.; Ōkawa, H.; Re, N.; Gallo, E.; Floriani, C. *Angew. Chem.* **1995**, *107*, 1565.

Scheme 1

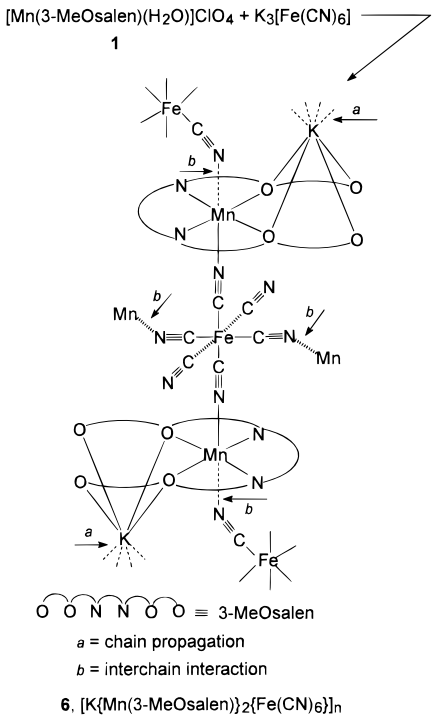

Scheme 2

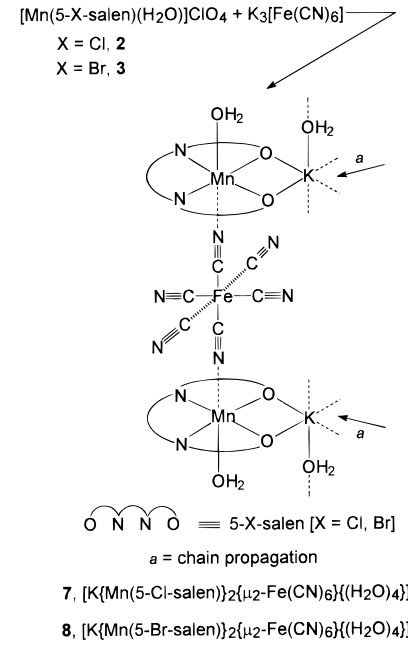

either as a powder, when the MeOH−H_2O solutions were mixed, or as crystals by a diffusion method (see the Experimental Section).

Powder and crystals of the same compound will be identified, when both exist, as P and C. Data pertaining to unsubstituted salen with the chemical formula $[Mn(salen)]_3[Fe(CN)_6]$ are reported only in the supporting information, since it produces a cocrystallized mixture of the anionic trimeric unit present in **6**−**8**, free $[Fe(CN)_6]^{3-}$, and $[Mn(salen)(H_2O)(MeOH)]^+$ and $[Mn_2(salen)_2(H_2O)_2]^{2+}$ as countercations, as confirmed by the X-ray analysis. The structural and magnetic properties are not particularly relevant in the present context. These data are given in the supporting information. Compounds **6**−**10** have been analytically characterized. The single C≡N band at 2118 cm^{-1} in $[Fe(CN)_6]^{3-}$ is split into two bands [**6**: 2114 and 2097 cm^{-1}]

Scheme 3

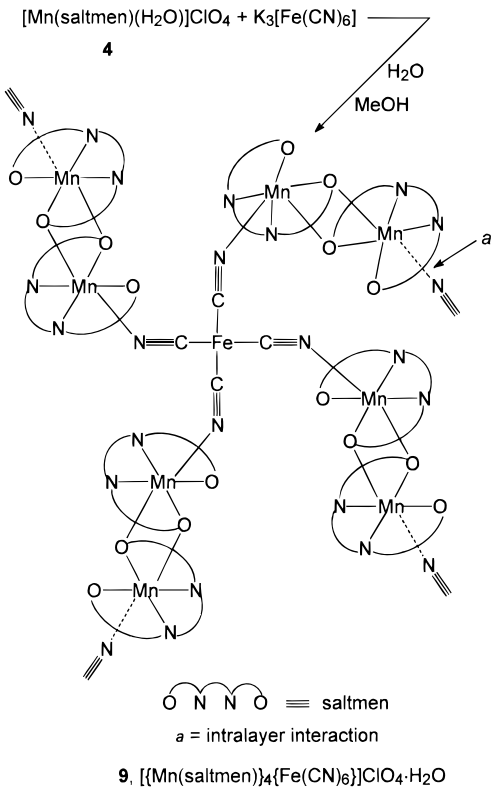

Scheme 4

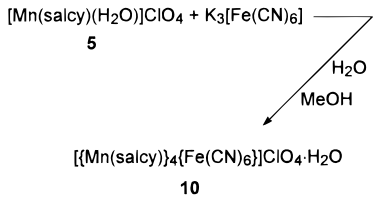

and three bands [**7**: 2129, 2114, and 2104 cm^{-1}] in the complexes formed, while a single band was observed in the IR spectrum for **9** [2118 cm^{-1}] and **10** [2112 cm^{-1}].

Structural Studies. Two structural classes of compounds are generated from the reaction between $[Mn(BS)(H_2O)]ClO_4$ and $K_3[Fe(CN)_6]$, and these are identified from the Mn:Fe ratio as the 2:1 and 4:1 compounds, respectively. Compounds **6**−**8** belong to the first class, and **9** and **10** to the second one.

The structural motif in the first class is the trimeric anion shown in Schemes 1 and 2. It can be considered as the building block of different polymeric structures depending on the arrangement of the countercation K^+ and the crystallization solvent. The structure of **6** will serve as an example when discussing the structures of **7** and **8** for which data are not available. An ORTEP view of the trimeric anion in **6** is shown in Figure 1, while the relevant structural parameters are reported in Table 1. Iron and potassium occupy the special positions (the inversion centers, Fe (1/2, 0, 1/2) and K (1/2, 0, 0)). The chains are made up by the trimers shown in Figures 2 and 3 bridged by K cations which are surrounded by the two O_4 sets of two adjacent trimers. The coordination environment of K^+ cations and the K−O distances (Table 1) are very close to those found in crownether−K complexes. The $[Fe(CN)_6]^{3-}$ building block assures both the intra- and the interchain linkages. It contains three different pairs of CN ligands, two terminals, and two intrachain and two interchain bridgings. We should mention that the Fe−C distances are slightly shorter in the intrachain bridging CN, but are very close for the other CN bonding modes.

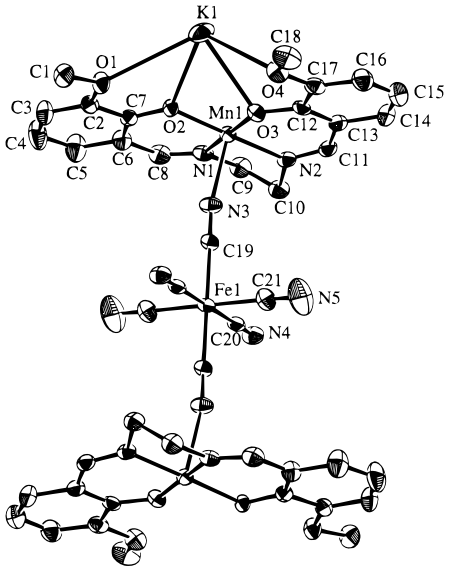

Figure 1. ORTEP drawing of a trinuclear structure for **6** with the numbering scheme of the unique atoms, showing 50% probability ellipsoids.

Table 1. Relevant Bond Distances (Å) and Angles (deg) for **6C**

Mn−N1	1.985(5)	Mn−N2	1.954(5)
Mn−N3	2.290(5)	Mn−N4*	2.415(5)
Mn−O2	1.868(4)	Mn−O3	1.878(4)
Fe−C19	1.932(5)	Fe−C20	1.943(6)
Fe−C21	1.941(7)	C19−N3	1.150(7)
C20−N4	1.157(7)	C21−N5	1.142(8)
K−O1	3.211(4)	K−O2	2.721(4)
K−O3	2.789(4)	K−O4	3.109(4)
Mn−K	3.5462(9)		
N1−Mn−N3	91.9(2)	N1−Mn−N4*	87.3(2)
N2−Mn−N3	89.4(2)	N2−Mn−N4*	84.4(2)
N3−Mn−N4*	173.8(2)	O2−Mn−N3	94.4(2)
O2−Mn−N4*	91.8(2)	O3−Mn−N3	93.2(2)
O3−Mn−N4*	87.2(2)	C19−Fe−C20	86.4(2)
C19−Fe−C21	92.2(2)	C20−Fe−C21	92.9(2)
O1−K−O2	50.4(1)	O1−K−O4	62.8(1)
O2−K−O3	58.5(1)	O3−K−O4	51.5(1)
Mn−N3−C19	169.5(5)	Mn−N4*−C20*	137.2(4)
Fe−C19−N3	177.2(5)	Fe−C20−N4	178.4(6)
Fe−C21−N5	177.5(6)		

The Mn−N distances are much longer in the interchain [Mn*−N4, 2.415(5) Å] [the asterisk indicates a symmetry operation of x, $1/2 - y$, $1/2 + z$] vs the intrachain interaction [Mn-N3, 2.290(5) Å]. The C−N bond distance is only slightly affected by the bonding mode, the terminal ones having the shortest bond at 1.142(8) Å. An additional structural parameter for understanding the interchain interactions is the C−N−Mn angle, varying from being almost linear for the intrachain bonding [Mn1−N3−C19, 169.5(5)°] to an interchain value of 137.2(4)° for Mn−N4*−C20*. Such Fe−C-N-Mn interactions produce a two-dimensional network having a repeating cyclic octameric $[(-Mn-NC-Fe-CN-)]_4$ unit. The center of the octameric ring is occupied by the KO_8 sandwich. Figures 2b and 3b show the two-dimensional layers stacking along the *a* axis and the interaction between the layers, assured by van der Waals contacts. The DMF molecules of crystallization fill the interlayer spaces. We should emphasize that the building up of the chains is assured by the availability of four oxygens *per* each [Mn(3-MeOsalen)] fragment complexing the alkali metal cation. Thus, the alkali metal cation is ordering the chain to make possible the interchain interaction *via* a rather long Mn−N interaction. In the case of **7** and **8**, which contain [Mn(5-X-salen)] with two oxygens only, the complexation of K^+ is completed either by solvent molecules, as we propose, or by oxygens of adjacent chains. This should not allow a regular interchain Fe−C−N−Mn interaction. This is supported by the magnetic properties of **7** and **8** which are, as expected for isolated trimeric units, not assembled in layers by significant Fe−C−N−Mn interactions. The assembling mode of the $[Mn(BS)(H_2O)]^+$ with $[Fe(CN)_6]^{3-}$ seems to depend largely on the steric characteristics of the cation. The nature of the Schiff base can determine the occurrence in solution of a prevailing monomeric or dimeric form of the cation (see forms **A** and **B** in eq 1). Compounds **6**−**8** are formed as a result of the assembly of the monomeric cation with $[Fe(CN)_6]^{3-}$, while in the case of **9** assembly occurs with the dimeric cation $[Mn_2(saltmen)_2(H_2O)_2]^{2+}$. In the case of a monomeric cation, the two axial positions of the Mn atom cannot be filled by two equally strong π-bonding CN groups because (i) two CN^- groups *trans* to each other will exert a self-labilization of one on the other and (ii) the manganese prefers the penta- vs the hexacoordination. In the case of a dimeric cation the two axial positions are equally available for binding with CN^- from $[Fe(CN)_6]^{3-}$. The consequence of those facts is the structure revealed by an X-ray analysis on **9**.

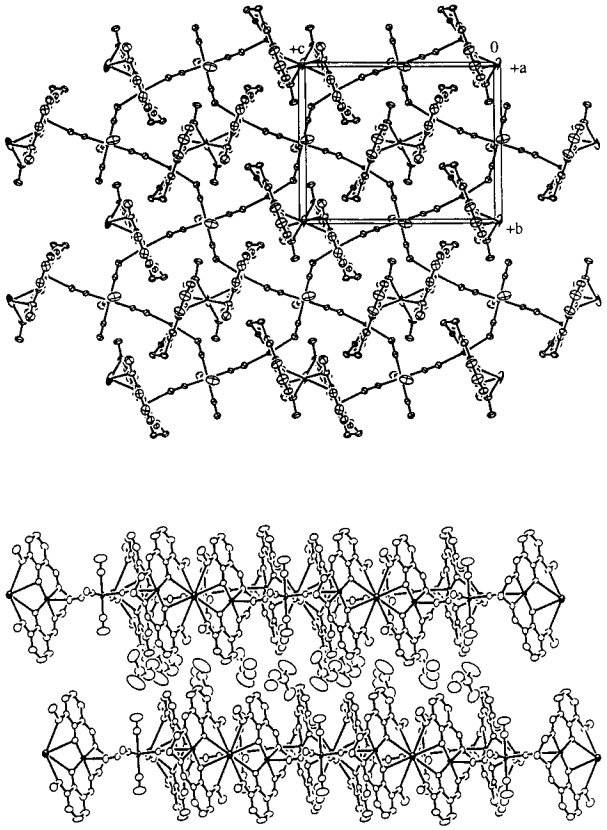

Figure 2. (top) Projection along the *a* axis for **6**, showing a two-dimensional network structure, in which a net unit is composed of a cyclic octamer structure $[(-Mn-NC-Fe-CN-)]_4$ and involves a sandwich structure. (bottom) Projection perpendicular to the *a*-axis, showing a stacking of the layers by van der Waals contact, where DMF molecules of crystallization fill the interlayer space.

The systematic absences of the reflection data of **9** cannot determine the space group unequivocally, with only the *I*4/*m* space group giving a satisfactory result. Figure 4 shows an ORTEP drawing of the pentanuclear cation $\{[Mn(saltmen)]_4[Fe(CN)_6]\}^+$ while relevant interatomic bond distances and angles are given in Table 2. The Fe and two cyanide groups lie on a 4-fold rotation axis (0, 0, z). The Fe is coordinated octahedrally by six CN^- groups, in which each of the four

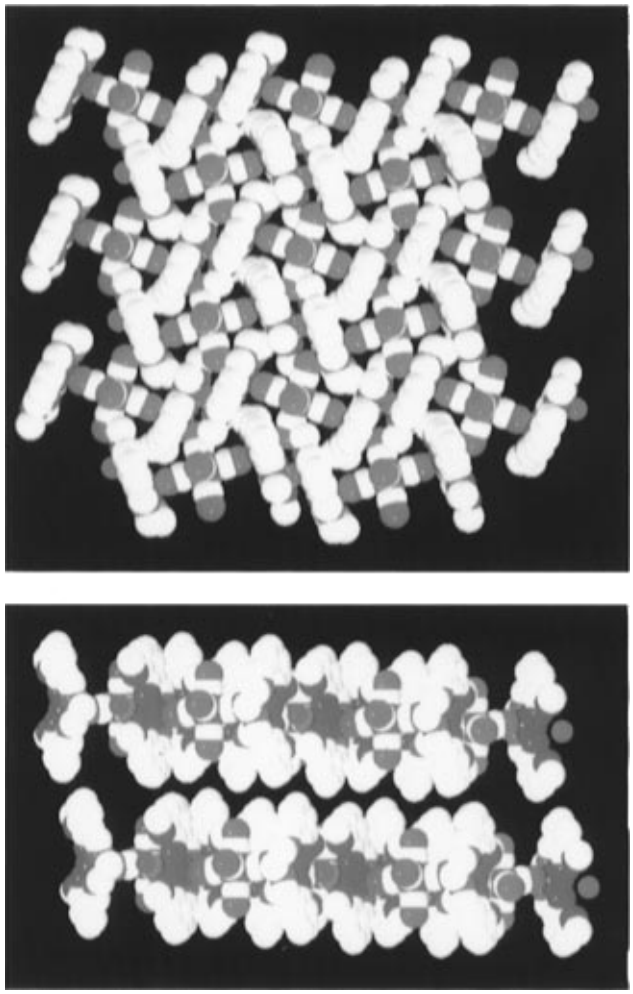

Figure 3. Space-filling representation of the two-dimensional network structure for **6**: (top) projection on the layer, (bottom) packing of layers, where DMF molecules are omitted for clarity.

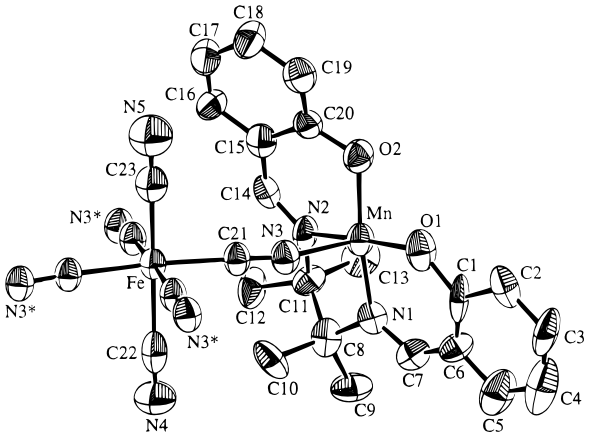

Figure 4. ORTEP drawing of unique atoms of a pentanuclear unit for **9** with the atom numbering scheme, showing 50% probability ellipsoids.

equatorial CN^- ligands coordinates axially to a Mn from a [Mn(saltmen)] moiety. This occurs in pairs *via* the sharing of an oxygen from the Schiff base. The coordination geometry around the Mn(III) ions is a distorted square bipyramidal geometry, in which the equatorial sites are occupied by the N_2O_2 donor atoms of the saltmen ligand while the two apical sites are occupied by the nitrogen atom N(3) of the CN^- and the phenoxy oxygen atom O(2)* of the adjacent unit (the asterisk indicates a symmetry operation of $1/2 + x$, $1/2 + y$, z) with a distance of Mn−O(2)* (phenoxy oxygen) = 2.847(9) Å.

Table 2. Relevant Bond Distances (Å) and Angles (deg) for **9C**

Mn−O1	1.877(9)	Mn−O2	1.894(10)
Mn−N1	1.94(1)	Mn−N2	1.97(1)
Mn−N3	2.19(1)	Fe−C21	1.94(1)
Fe−C22	2.11(4)	Fe−C23	1.84(3)
N3−C21	1.14(2)	N4−C22	1.08(5)
N5−C23	1.14(5)		
O1−Mn−N3	96.0(4)	O2−Mn−N3	94.9(4)
N1−Mn−N3	99.7(5)	N2−Mn−N3	90.0(4)
C21−Fe−C22	88.4(5)	C21−Fe−C23	91.6(5)
Fe−C21−N3	175(1)	Fe−C22−N4	180.0
Fe−C23−N5	180	Mn−N3−C21	156.1(10)

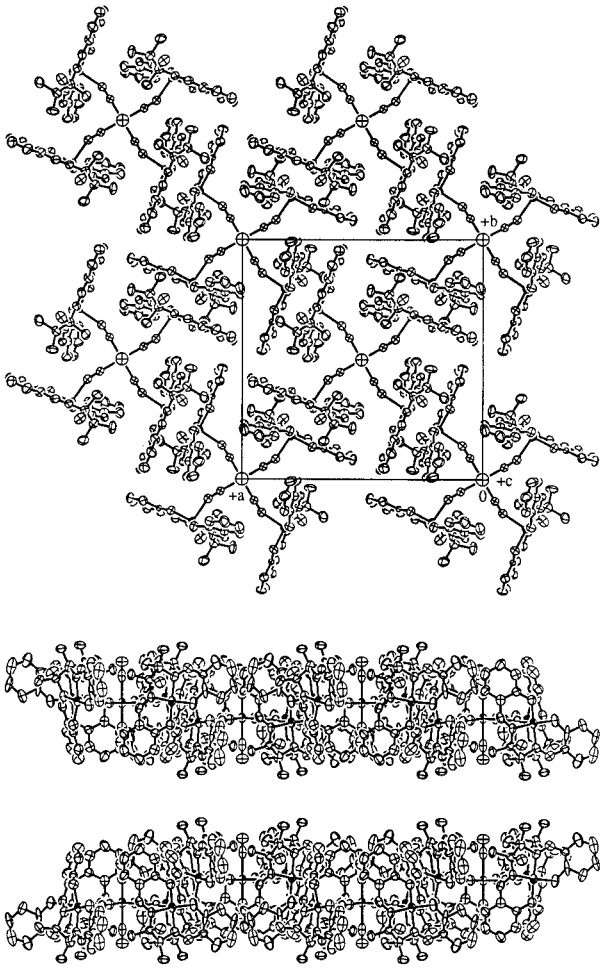

Figure 5. (top) Projection along the *c* axis of **9**, showing a two-dimensional network structure, in which the out-of-plane structure between $[Mn(saltmen)]^+$ ions is composed and a net unit is composed of a cyclic octamer structure $[(\cdots Mn-NC-Fe-CN-Mn\cdots)]_4$. (bottom) Projection perpendicular to the *c*-axis, showing a stacking of the sheet structure by van der Waals contact.

A crystal structure, projected on the *ab*-plane, is given in Figures 5a and 6a, and shows the two-dimensional network structure. A projection of the structure along the *c*-axis is given in Figures 5b and 6b and illustrates the stacking of the layer structure, with perchlorate ions positioned between the layers.

The formation (see Scheme 4) of **10** involves the same stoichiometry as that of **9**. This may suggest a close structural relationship between the two compounds. However, in this case, the magnetic measurements were very diagnostic and showed the difference between the two species and also the absence of any extended structure for **10**. The magnetic measurements are in favor of the presence of the trimeric form shown for compounds **6**−**8** and noninteracting cations. Some preliminary X-ray data obtained for the structure made by the separated ions

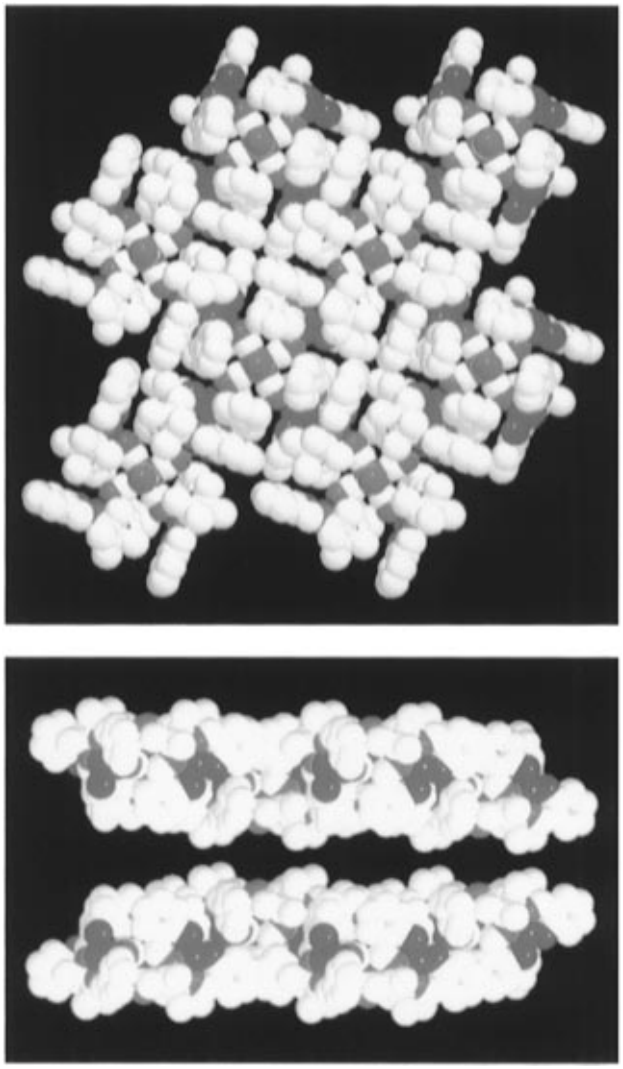

Figure 6. Space-filling representation of the two-dimensional network structure for **9**: (top) projection on the layer, (bottom) packing of layers.

$\{Mn(salcy)\}_2\{Fe(CN)_6\}^-$, 2 $[Mn(salcy)(H_2O)_2]^+$, and ClO_4^- confirmed this. Once again steric factors associated with the Schiff base determine the assembly mode. In the case of salcy, the particularly hindered cyclohexyl substituent prevents both the formation of the manganese derivative in a dimeric form and any intertrimer interactions.

Magnetic Properties. We have studied the temperature dependence of the magnetic susceptibility in the temperature range 1.9−300 K for compounds **6**−**10**. The results of these measurements indicate different behaviors for compounds **7**, **8**, and **10** with respect to **6** and **9**. Indeed the former compounds behave as isolated oligomers, while the latter show the occurrence of a spontaneous magnetic ordering due to the magnetic phase transition at low temperature which reflects their extended structure. For these latter compounds further measurements of the temperature and field dependence of the magnetization have been performed.

Compounds with Isolated Oligomeric Structure. Compounds 7 and 8. Since the magnetic behaviors of **7** and **8** are quite similar, only the behavior of **7** will be described. The temperature dependence of the effective magnetic moment μ_{eff} per Mn_2Fe unit for **7**, together with that of **6**, is shown in Figure 7. The μ_{eff} at room temperature, 7.31 μ_B, is slightly larger than the spin-only value of 7.14 μ_B for the magnetically dilute three-spin system (S_{Mn}, S_{Fe}, S_{Mn}) = (2, 1/2, 2), where the spin-only

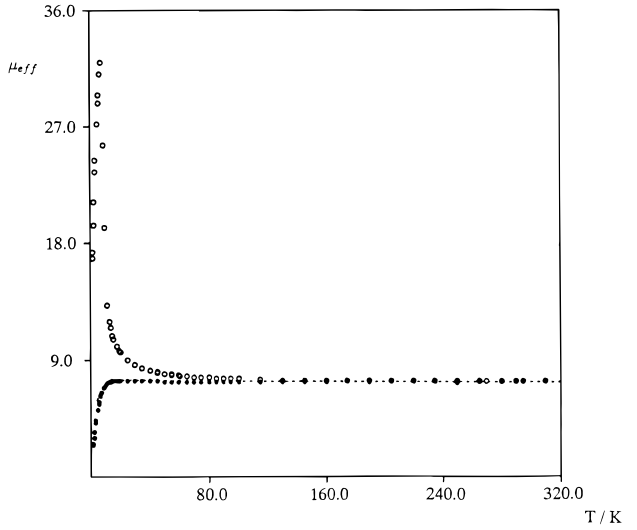

Figure 7. Effective magnetic moment for **6** (○) and **7** (●) per Mn_2Fe vs temperature. The dashed line represents the calculated curve for **6** using the Hamiltonian shown in eq 2 and the best fit parameters g_{Mn} = 2.04, g_{Fe} = 2.04, J = +4.2 cm^{-1}, zJ' = −0.3 cm^{-1}, and D = −7.8 cm^{-1}.

value was calculated by assuming g values of g_{Mn} = 2.00 and g_{Fe} = 2.00. As the temperature is lowered, the magnetic moment gradually increases to reach a maximum of 8.5 μ_B at 20.2 K, and then decreases sharply. The decrease of μ_{eff} at low temperature is due to the zero-field splitting term of the manganese(III) ion and/or an intermolecular antiferromagnetic interaction. The magnetic susceptibility data can be fitted by the spin-Hamiltonian (eq 2) based on the symmetrical linear

$$H = \beta H(2g_{Mn}S_{Mn} + g_{Fe}S_{Fe}) - [S_{Mn1}S_{Fe} + S_{Mn2}S_{Fe}] + D[S_{z^2} - (1/3)S_{Mn}(S_{Mn} + 1)] - zJ'S\langle S\rangle \quad (2)$$

trinuclear structure of Mn(III)−Fe(III)−Mn(III) with the spin-system of (S_{Mn}, S_{Fe}, S_{Mn}) = (2, 1/2, 2) including a zero-field splitting term and an inter-molecular interaction term within the molecular field approach, where the magnetic interaction between the terminal Mn ions is neglected.

The susceptibility for such a system is calculated using the thermodynamic relationship χ = M / H, where

$$M = [N\sum_i(-dE_i/dH)\exp(-E_i/k_BT)]/[\sum_i\exp(-E_i/k_BT)] \quad (3)$$

The energy levels of the trimer, E_i, are evaluated by diagonalizing the Hamiltonian matrix in the basis constituted by the product of the spin functions for the single (2, 1/2, 2) spin centers.

The best fit parameters are J = +4.2 cm^{-1}, zJ' = −0.3 cm^{-1}, g_{Mn} = 2.04, g_{Fe} = 2.04, and D = −7.8 cm^{-1} for **7** and J = +4.5 cm^{-1}, zJ' = -0.3 cm^{-1}, g_{Mn} = 2.02, g_{Fe} = 2.00, and D = −8.5 cm^{-1} for **8**. Actually, it is not possible from these data on polycrystalline samples to distinguish between positive and negative D values, but negative signs have been assumed on the basis of magnetization data (*vide infra*) and also because negative D values of a few cm^{-1} are typical for Mn(III) Schiff base complexes.[15] The above parameters indicate an intramolecular ferromagnetic coupling between Mn(III) and Fe(III) ions, a weak intermolecular antiferromagnetic interaction, and a large zero-field splitting. The theoretical μ_{eff} vs T curve for **7** using the best-fit parameters is represented by the dashed line in Figure

(15) Kennedy, B. J.; Murray, K. S. *Inorg. Chem.* **1985**, *24*, 1552.

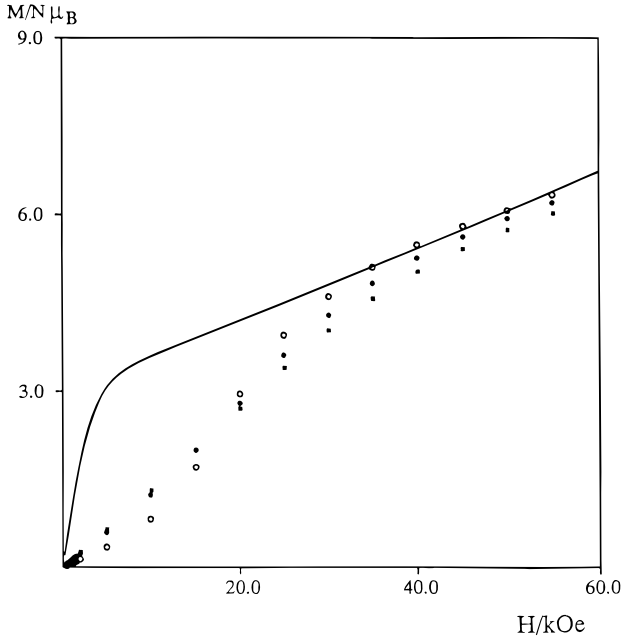

Figure 8. Magnetization as a function of the applied magnetic field for **7**, performed at 1.9 K (○), 4.5 K (■), and 6.0 K (●). Solid line at 1.9 K represents a theoretical curve.

7. The field dependences of the magnetization of **7** measured at 1.9, 4.5, and 6.0 K are shown in Figure 8 in the form of $M/N\mu_B$ vs H plots (where M, N, μ_B, and H are magnetization (cm^3 mol^{-1} Oe), Avogadro's number, the electron Bohr magneton, and the applied magnetic field (Oe)). On increasing the applied magnetic field at 1.9 K, the magnetization value increases gradually showing an almost linear dependence above 30 K. An analogous behavior is shown by **8**. This behavior is typical of systems with a relevant anisotropy due to a large zero-field splitting and is consistent with the high value of -7.8 cm^{-1} for D, found for the Mn(III) ion by the fitting of μ_{eff} vs T. A semiquantitative fitting of magnetization vs H can be obtained on the basis of the following considerations. First of all, we note that, for the value $J = +4.2$ cm^{-1} found from the fitting of μ_{eff}, the trimer unit is expected to have an $S = 9/2$ ground state thermally isolated, at least at 1.9 K, from the first $S = 7/2$ excited state. For such an isolated ground state, the variation of the magnetization with the field would follow the Brillouin function with saturation to a value of ca. $9N\mu_B$. However, in the presence of a splitting of the spin multiplet due to zero-field splitting, the magnetization increases more slowly, reaching the saturation value at much higher fields. The magnetization for such a system may be calculated by using eq 3.

The energy levels are obtained through a full matrix diagonalization employing the 10 spin functions of the $S = 9/2$ state and the effective axial spin Hamiltonian $H = \beta g_z H_z S_z + \beta g_x (H_x S_x + H_y S_y) + D[S_z^2 - S(S+1)/3]$, where we assume $g_z = g_x = g$, and g and D are the effective g factor and the zero-field splitting, respectively, for the $S = 9/2$ state and can be related through the Wigner−Eckart theorem to the single ion values g_{Mn}, g_{Fe}, and D_{Mn}.[16] In particular if $g_{Mn} = g_{Fe}$, as observed in our case, $g = g_{Mn} = g_{Fe}$, while it is straightforward to show that $D = (1/3)D_{Mn}$. Taking into account that the Zeeman energy is on the order of $\mu_B H$, intermolecular interactions on the order of 0.5 cm^{-1} would affect magnetization up to 20-30 kOe. Thus, we discarded the experimental data at low fields, taking only the data above 30 kOe. A reasonably good fit for the magnetization data at 1.9 K at fields above 30 kOe is obtained for $g = 2.0$ (fixed to the value obtained in the μ_{eff} fit) and $\mathbf{D} = -1.3$ cm^{-1} (see Figure 8). This fit clearly indicates a negative D value, positive values being unable to reproduce the almost linear increase of M with H. The D value obtained from this fit, -1.3 cm^{-1}, would correspond to a D_{Mn} of about -4 cm^{-1} and is in reasonable agreement with the known data for other Mn(III) Schiff base complexes.[15] A slight discrepancy is observed with the value of D_{Mn} obtained from the μ_{eff} vs T fit, -7.8 cm^{-1}. However, it must be considered that in the fitt of μ_{eff}, the D and zJ' parameters were strongly coupled and are therefore both subjected to a relevant uncertainty.

The overall magnetic behavior of compounds **7** and **8** thus strongly supports their nature of magnetically isolated trimeric units, as suggested by structural considerations.

Compound 10. The plot of $1/\chi_M$ vs T obeys the Curie law ($1/\chi_M = C/T$), indicating no detectable magnetic interaction. The μ_{eff} at room temperature, 9.98 μ_B, is nearly equal to the spin-only value of 9.95 μ_B for the magnetically dilute five-spin system (four S_{Mn}, S_{Fe}) = (four 2, 1/2). On lowering the temperature, the μ_{eff} keeps constant and then decreases gradually at low temperatures. This behavior is compatible with the presence of a trimeric Mn−Fe−Mn unit and two non interacting Mn(BS) cations, as evidenced by preliminary X-ray results. The low temperature decrease of μ_{eff} could be due to the zero-field splitting of the Mn(III) ion and/or antiferromagnetic intermolecular interactions.

Compounds with Extended Structure. Compound 6. First, it should be noted that the magnetic measurements were performed both for a powder sample, **6P**, and a crystalline sample, **6C**. The magnetic behaviors for the two are very similar, but show a slight difference at low temperature and a weak magnetic field (below ca. 300 Oe). The μ_{eff} vs T curve of **6P**, taken under an external field of 800 Oe, is given in Figure 7 and shows a distinctly different magnetic behavior from the other 2:1 complexes **7** and **8**. The effective magnetic moment at room temperature, 7.33 μ_B, is slightly larger than the spin-only value, 7.14 μ_B, for the magnetically dilute three-spin system (S_{Mn}, S_{Fe}, S_{Mn}) = (2, 1/2, 2). The plot of $1/\chi_M$ vs T obeys the Curie−Weiss law with the positive Weiss constants of $\Theta = +6.8$ K. As the temperature is lowered, the μ_{eff} increases gradually and then sharply without a round minimum, reaches a maximum value of 32.1 μ_B at 9 K, and finally decreases abruptly to 17.4 μ_B at 1.9 K. The maximum value of μ_{eff} is significantly larger than that of the largest possible spin state, $S_T = 9/2$, for (S_{Mn1}, S_{Fe}, S_{Mn2}) = (2, 1/2, 2), $\mu_{so} = 9.95$ μ_B.

As elucidated by X-ray analysis, the two-dimensional layer structure is composed of a cyclic octamer, $[(-Mn-NC-Fe-CN)]_4$, involving a sandwich structure in which it should be considered that there are three possible magnetic paths between the magnetic metal ions. The first two interactions are intratrimer and intertrimer paths between Mn(III) and Fe(III) through a CN group. The magnetic behavior suggests that both interactions should be ferromagnetic. The absence of a round minimum in the curve of μ_{eff} vs T and the structural analogy of the trimer unit with that for compounds **7** and **8**, for which magnetic data have been fitted for an intratrimer ferromagnetic coupling constant, strongly support an intratrimer ferromagnetic path also in compounds **6P** and **6C**. The intertrimer path through a CN group within the planes must be ferromagnetic in order to explain the abrupt increase of μ_{eff} below ca. 20 K. Although we should also consider the third magnetic path, which involves the Mn(III) ions through the K^+ ion of the sandwich structure, the magnetic interaction through the K^+ ion, as well as that between the terminal manganese(III) ion through the NC−Fe−CN moiety, is negligible. This is confirmed by a study

(16) Bencini, A.; Gatteschi, D. *Electronic Paramagnetic Resonance of Exchange Coupled Systems*; Springer-Verlag: Berlin, Germany, 1990.

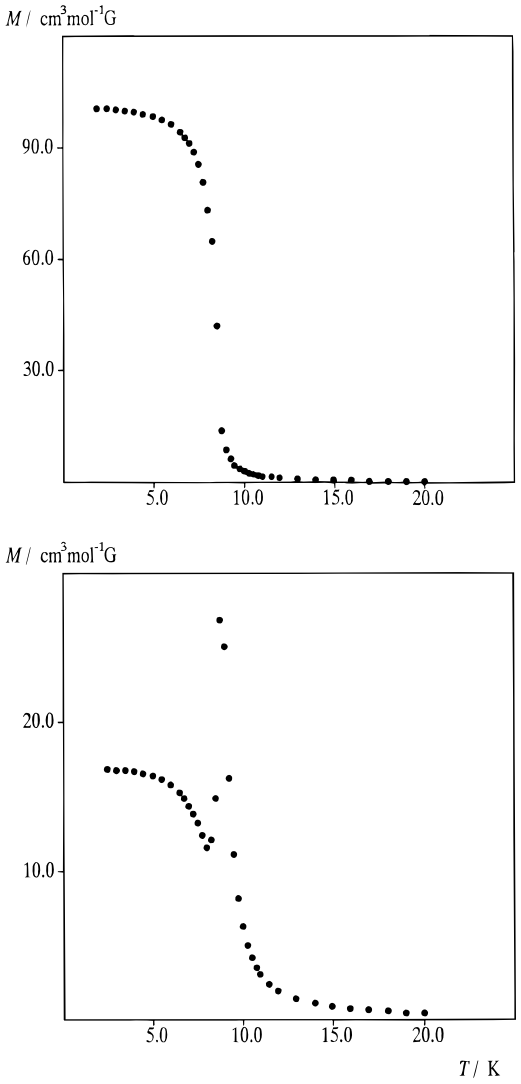

Figure 9. FCM (field-cooled magnetization) vs *T* curve under a weak magnetic field, 0.5 Oe, for (top) **6P** and (bottom) **6C**.

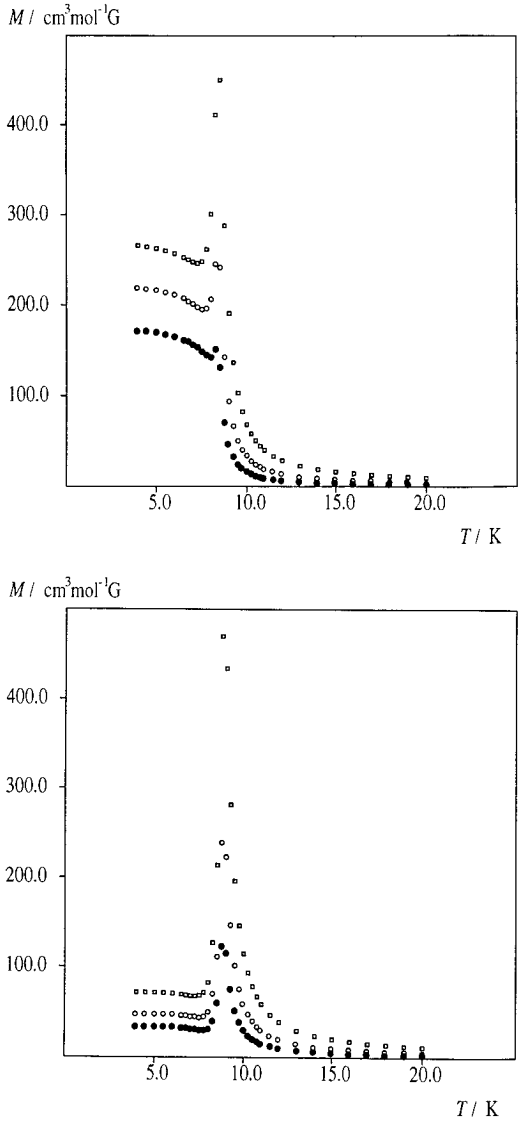

Figure 10. FCM (field-cooled magnetization) vs *T* curve under weak magnetic fields, 5 (●), 10 (○), and 20 (□) Oe, for (top) **6P** and (bottom) **6C**.

of the magnetic properties of the complexes for which cobalt(III) is substituted for the iron(III) ion of **6P** and **6C**. The X-ray diffraction pattern of powder and crystal samples of K[Mn(3-MeOsalen)]$_2$[Co(CN)$_6$] is isomorphous with respect to **6P** and **6C**. Since Co(III) is diamagnetic, the possible magnetic paths are limited to the two interactions described above. The plot of $1/\chi_M$ vs *T* almost obeys the Curie law, indicating no magnetic interaction, while the decrease of μ_{eff} at very low temperature is ascribed to the zero-field splitting of the Mn(III) ion. These results are consistent with a negligible magnetic interaction between Mn(III) ions through the K^+ ion and through the NC−Fe−CN moiety. Our experimental evidence agrees with the result of Pecoraro et al. who reported that the magnetic interaction between Mn(III) ions through an alkali metal ion is nondetectable on the basis of the magnetic properties of [NaMn$_2$(2-OHSALPN)$_2$(OAc)$_4$] (2-OHSALPN = *N*,*N*′-disalicylidene-*N*,*N*′-(2-hydroxypropylene)diamine).[17]

FCM (field-cooled magnetization vs *T*) curves of **6P** and **6C** were obtained by cooling the sample under a weak magnetic field, 0.5 Oe, and these results are shown in Figure 9. On lowering the temperature under a field of 0.5 Oe, the magnetization of **6C** shows a rapid increase below ca. 10 K, to reach a maximum at 9.2 K, and then decreases further, while that of **6P** showed no decrease after a rapid increase at ca. 8 K. Furthermore, the magnetization value obtained below 8 K of **6P**, ca. 100 cm^3 mol^{-1} G, is much higher than the maximum value of ca. 30 cm^3 mol^{-1} G observed for sample **6C**. In order to better understand the reasons for these different behaviors, FCM curves were taken for both **6P** and **6C** at magnetic fields of 5, 10, and 20 Oe and are given in Figure 10. We see that while the curves for **6C** are qualitatively similar to those observed under 0.5 Oe, those for **6P** are different, showing a very small cusp at ca. 8.2 K under 5 Oe, a small peak at ca. 8.5 K under 10 Oe, and a sharp peak at 8.9 K under 20 Oe. Moreover, increasing the applied field from 5 to 20 Oe causes the onset of a rapid increase of magnetization which begins at higher temperatures, ca. 8.5, 9, and 10 K, respectively. It is worth noting that the FCM curves under 20 Oe are essentially equivalent for the two samples, differing only in the value of magnetization at the plateau below the maximum, 260 cm^3 mol^{-1} G vs 70 cm^3 mol^{-1} G, for **6P** and **6C**, respectively. These characteristic FCM curves and the positive Weiss constant are consistent with a metamagnetic behavior.[18] The abrupt increase of the magnetization indicates the onset of long-range magnetic ordering due to the ferromagnetic coupling within each layer. The decrease below 9.2 K indicates the presence of interlayer antiferromagnetic interactions. However, the FCM curves in

(17) Bonadies, J. A.; Kirk, M. L.; Lah, M. S.; Kessissoglou, D. P., Hatfield, W. E.; Pecoraro, V. L. *Inorg. Chem.* **1989**, 28, 2037.

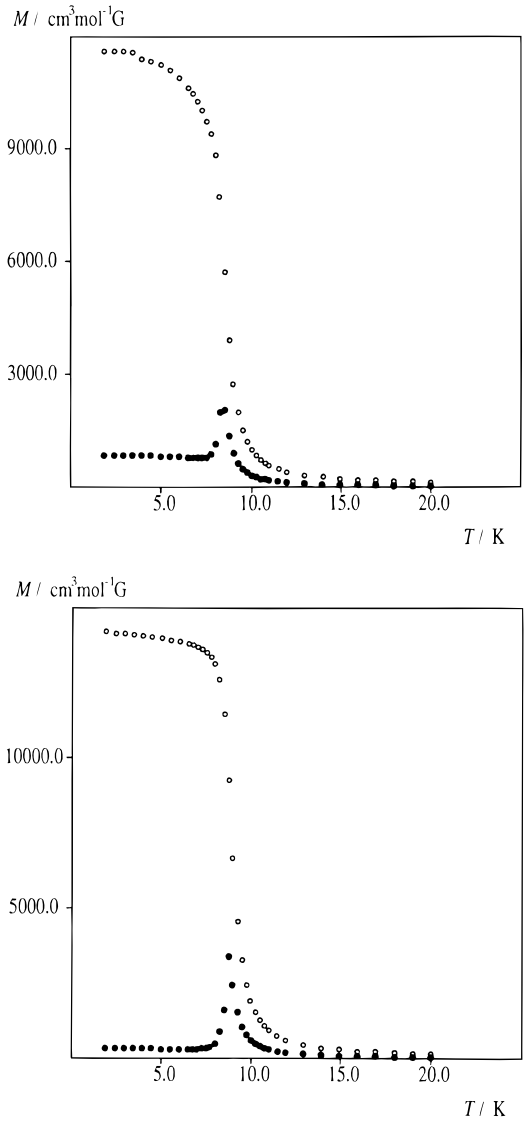

Figure 11. FCM (field-cooled magnetization) vs *T* curve under weak magnetic fields, 100 (●) and 300 (○) Oe, for (top) **6P** and (bottom) **6C**.

Figures 9 and 10 show that at temperatures below the sharp peak at 8.5−9.2 K the magnetic moment does not go to zero and even slightly increases. This latter behavior could be explained by a spin fluctuation mechanism. In other words, although the interlayer spins couple antiferromagnetically and the spins between adjacent layers should be antiparallel at temperatures below the peak, there are random fluctuations from this perfect arrangement which give rise to a resultant magnetization. Figure 11 shows the FCM curve measured under 100 and 300 Oe, for **6P** and **6C**. In both cases, the *M* vs *T* curve under 100 Oe still shows a sharp peak at 9.2 K, while the curve under 300 Oe has no peak and remains constant after the abrupt increase at ca. 9 K. This result implies that an external magnetic field of 300 Oe is high enough to overcome the antiferromagnetic interaction operating between the adjacent layers and to make the magnetic vectors parallel, but that 100 Oe is not. To confirm the metamagnetic transition, and better characterize the

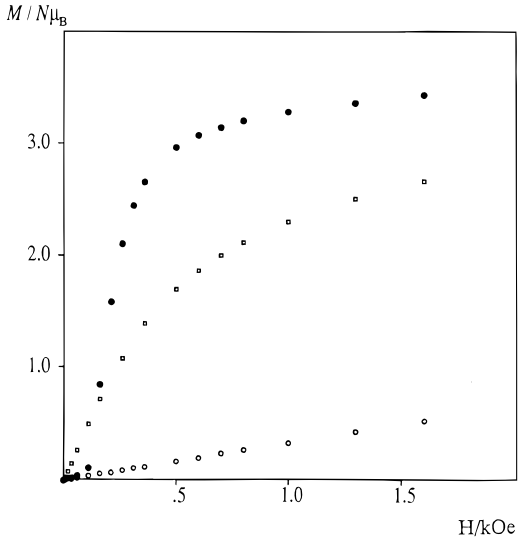

Figure 12. Magnetization as a function of the applied magnetic field for **6C**, performed at 6 K (●), 9 K (□), and 12 K (○).

antiferromagnetic to ferromagnetic transition, the magnetization was taken as a function of the external magnetic field at various temperatures below and above the Neel temperature. The results are reported in Figure 12 only for **6C**, as the curves for **6P** are very similar. Below 9.2 K, the curves have a sigmoidal behavior: the magnetization first increases slowly with H, as for a typical antiferromagnet, and then increases abruptly, showing a phase transition to a ferromagnetic state, as expected for a metamagnet. The critical field for the lowest temperature of 2 K is almost 300 Oe; as the temperature is raised, the phase transition shifts to lower fields and finally disappears for temperatures above T_N, still confirming metamagnet behavior. Hysteresis loops have been observed for **6P** and **6C**, and those measured at 4.5 K are given in Figure 13. This confirms that the interlayer antiferromagnetic coupling does not lead to a fully antiparallel orientation of the spins below the Neel temperature. These hysteresis loops show a metamagnetic character in the virgin magnetization procedure and a slight difference between the two samples. The field dependence of the magnetization up to 55 kOe on the powder sample **6P** was measured at 4.2, 6.0, and 7.5 K, and the results are given in Figure 14. On increasing the applied magnetic field at 2 K, the magnetization value is nearly zero below ca. 250 Oe, increases rapidly to a plateau (ca. $M = 3N\mu_B$) around 1500 Oe, and then increases linearly to $6N\mu_B$ at 55 kOe. Since the saturation magnetization M_s is expected to be $9N\mu_B$ for the system (S_{Mn}, S_{Fe}, S_{Mn}) = (2, 1/2, 2) on the basis of the equation $M_s = Ng\mu_B S$, a higher magnetic field than 55 kOe is necessary for the magnetic saturation of this compound. This behavior can be easily interpreted in a manner simlar to that above for the magnetization curves of compound **7**, taking into account the large zero-field splitting effect. Due to the similar trimeric structure, **6C** is expected to have intratrimer parameters *J* and D_{Mn} similar to those for **7**. We would expect an isolated $S = 9/2$ ground state with an effective *D* of about -1.5 cm^{-1}, as the trimer contribution to the magnetization curve at high fields is anticipated to be similar to that shown in Figure 8 for compound **7**. Therefore, the trimer contribution to the *M* vs *H* curve at low temperaures is expected to reach a value of about $3N\mu_B$ at about 10 kOe, and then to increase linearly up to ca. $6N\mu_B$ at 55 kOe. Due to the strong intertrimer ferromagnetic interactions within the layers, the plateau is reached immediately after the metamagnetic transition at 200−300 Oe. The magnetization then increases linearly and could be interpreted analogously through the full

(18) (a) Carlin, R. L. *Magnetochemistry*, Springer-Verlag, Berlin, Germany, 1986. (b) Kahn, O. In *Magneto-Structural Correlations* In *Exchanged Coupled Systems*; Gatteschi, D., Kahn, O., Willett, R. D., Eds.; Reidel: Dordrecht, The Netherlands, 1985. (c) Carlin, R.; vanDuyneveldt, A. *Acc. Chem. Res.* **1980**, *13*, 231. (d) De Fotis, G. C.; McGhee, E. M.; Bernal, I.; Losee, D. B. *J. Appl. Phys.* **1987**, *61*, 3298. (e) Smart, J. S. *Effective Field Theories of Magnetism*; Saunders: Philadelphia, 1966.

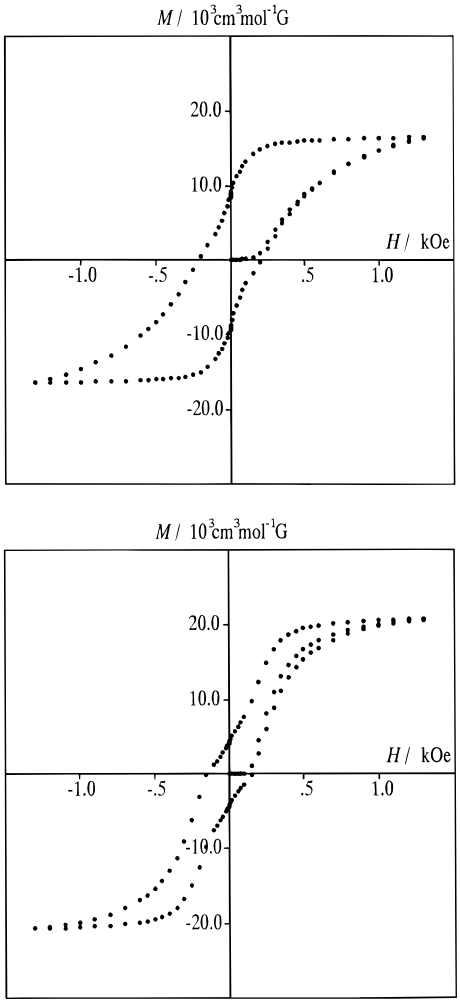

Figure 13. Hysteresis loop ($M/N\mu_B$ vs H) at 4.5 K for (top) **6P** and (bottom) **6C**. The remnant magnetization is 5000 cm^3 mol^{-1} G, and the coercive fields is 400 and 200 G, respectively.

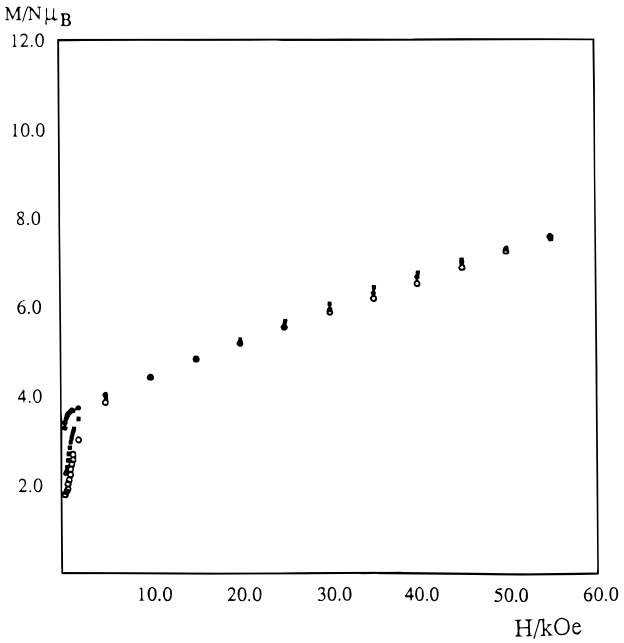

Figure 14. Magnetization as a function of the applied magnetic field for **6P**, performed at 2 K (○), 4.5 K (■), and 6 K (●).

matrix diagonalization technique and the effective axial spin Hamiltonian (eq 2). It is therefore the strong anisotropy of the Mn(III) ion which prevents the compound from reaching the

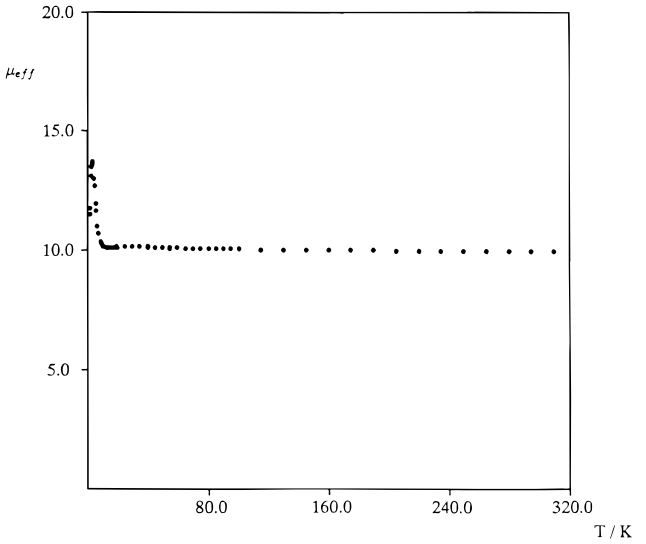

Figure 15. Effective magnetic moment for **9** per Mn_4Fe against temperature.

expected saturation value of $9N\mu_B$ at 55 kOe. This interpretation also agrees with the metamagnetic nature of compounds **6P** and **6C**, as it is well known that metamagnetism is usually associated with a large anisotropy.[18]

Another interesting point to note is that the magnetization saturates more easily as the temperature increases (see Figure 14). These behaviors are consistent with a metamagnetic character,[18] where within each layer the coupling between magnetic metal ions is ferromagnetic and the coupling between the layers is antiferromagnetic. The interlayer antiferromagnetic interaction is expected to be very weak due to the van der Waals contacts, where DMF molecules are positioned between the layers as a crystallization solvent. It is also envisaged that the DMF molecules affect the interlayer antiferromagnetic interaction and also the spin fluctuation mechanism mentioned above. Therefore, the magnetic difference below 300 Oe between the two samples **6P** and **6C**, which have been prepared by different methods, can be ascribed to a slight difference in the interlayer interaction between them. Moreover, the higher magnetization value observed for **6P** at the plateau below the peak in the FCM curves (see Figure 10) clearly indicates weaker interlayer antiferromagnetic interactions.

Compound 9. The magnetic properties of samples **9P** and **9C** are quite similar, and only the behavior of **9P** will be described. The μ_{eff} vs T curve of **9** is shown in Figure 15. The plot of $1/\chi_M$ vs. T obeys the Curie−Weiss law with a positive Weiss constant of $\Theta = +2.8$ K. The μ_{eff} of **9** at room temperature, 9.83 μ_B, is nearly equal to the spin-only value of 9.95 μ_B for the magnetically dilute five-spin system (four S_{Mn}, S_{Fe}) = (four 2, 1/2). As the temperature is lowered, μ_{eff} increases gradually and then sharply without a minimum, reaching a maximum value of ca. 14 μ_B at 4.4 K, and finally decreases to ca. 12 μ_B at 1.9 K. The sharp increase at low temperatures would suggest a ferromagnetic interaction and three-dimensional magnetic ordering.

To confirm the magnetic phase transition, the magnetization M vs T was investigated in zero and weak magnetic fields. The results are represented in Figure 16. The FCM (field-cooled magnetization vs T) curve was obtained by cooling the sample under a weak magnetic field, 0.5 Oe, and shows a rapid increase below ca. 5 K and a break in the curve around $T_c = 4.5$ K. When the field was switched off at 1.9 K, remnant magnetization was observed. The remnant magnetization vanishes at the T_c upon warming. Finally, the zero-field-cooled magnetization

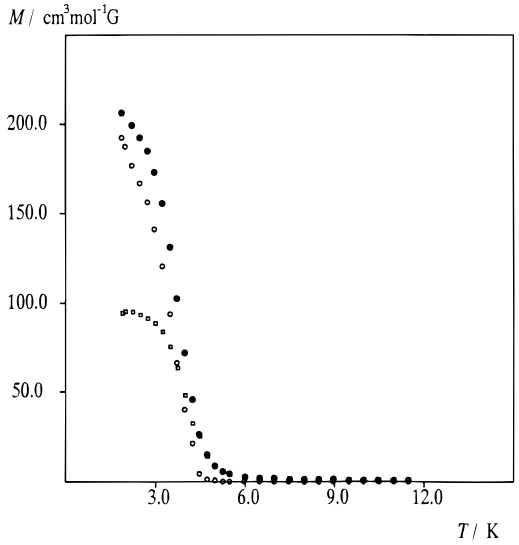

Figure 16. Temperature dependence of the magnetization M for **9** under 0.5 G: field-cooled magnetization (○), remnant magnetization (●), zero-field magnetization (□).

(ZFCM), obtained by cooling in zero field and warming under the field, was measured. It is very similar to the FCM curve, probably because above 1.9 K, the domain wall dynamics are very fast. All of these features are characteristic of a ferromagnetically ordered state below 4 K.[1,5]

The hysteresis loop at 4.5 K is shown in Figure 17 and displays a characteristic behavior for a ferromagnet with a coercive field of about 80 Oe and a remnant magnetization of 1800 $cm^3\ mol^{-1}$ G. The field dependence of the magnetization up to 55 kOe was measured at 1.9, 4.5, and 6.0 K, and the results are shown in Figure 18. On increasing the applied magnetic field at the lowest temperature of 1.9 K, the magnetization value increases gradually. Note that the slope of this magnetization curve in the limit of zero field (see Figure 18) is smaller than that of typical ferromagnets and also that, at higher fields, the increase of magnetization is very slow. The saturation magnetization M_s is expected to be 17 $N\mu_B$ for this five-spin system (four S_{Mn}, S_{Fe}) = (four 2, 1/2) on the basis of the equation $M_s = Ng\mu_B S$, but the observed magnetization only reaches $10.3N\mu_B$ at 55 kOe. Magnetic fields higher than 55 kOe are therefore necessary for the magnetic saturation of this compound. This can be interpreted in a way similar to that for compounds **7**, **8**, and **6** by taking into account the large zero-field splitting of the Mn(III) ions within the pentamer units. It should be noted that the magnetization saturates more easily as the temperature decreases, as seen in Figure 18. This tendency, which is opposite that observed for the metamagnetic **6C**, also supports the ferromagnetism of compound **9**.

The above magnetic behavior shows that the intralayer and interlayer magnetic interactions are both ferromagnetic. Since complex **9C** assumes a two-dimensional layer structure with a net unit of a cyclic dodecamer $[(-NC-Fe-CN-Mn\cdots Mn-)]_4$, the magnetic interactions between the Fe(III) and Mn(III) ions through the CN^- group, as well as that between the two Mn(III) ions in the out-of-plane dimeric unit, must both be ferromagnetic. Such an out-of-plane dimer structure is well known for a number of manganese(III) complexes with the salen analogues. Although the most cases a small antiferromagnetic interaction is observed,[15,17] a ferromagnetic interaction is also known for a few other complexes.[19] The Mn−O distance of the Mn_2O_2 dimeric core is 2.847(9) Å, which is substantially longer than for the related manganese(III) complexes exhibiting antiferromagnetic coupling. The ferromagnetic interaction is experimentally confirmed by the magnetic measurement of the cobalt(III) substitute which is the isomorph of the iron(III) compound. On lowering the temperature, the effective magnetic moment per Mn increases from ca. 4.5 to 5.0 μ_B, indicating a ferromagnetic interaction of the out-of-plane dimeric unit.

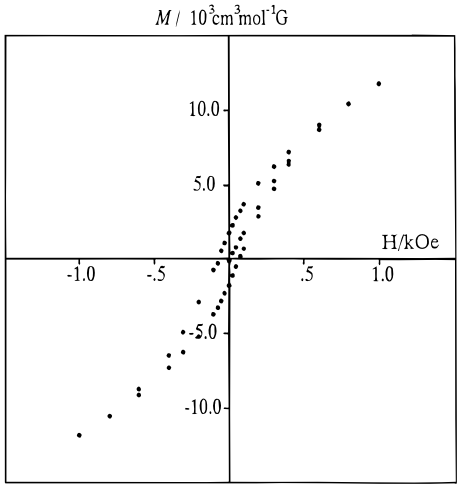

Figure 17. Hysteresis loop ($M/N\mu_B$ vs H) at 4.5 K for **9**, in which the remnant magnetization is 1800 $cm^3\ mol^{-1}$ G and the coercive field is 80 Oe.

Magnetostructural Correlation. The magnetic interaction between various combinations of two magnetic centers A and B with a CN^- group has been examined experimentally and theoretically.[20]

In the simplest orbital scheme of exchange between two magnetic centers, A and B,[21] the coupling constant J can be given by the equation

$$J = \frac{1}{n_A n_B} \sum_{i,j} J_{ij}$$

where J_{ij} is the contribution due to the interaction between the magnetic orbitals i on A and j on B, and n_I is the number of unpaired electrons on center I (I = A,B).

In general, the pair contributions J_{ij} can be written as the sum of a ferromagnetic term, $J_{ij}^F > 0$, and an antiferromagnetic term, $J_{ij}^{AF} < 0$, as $J_{ij} = J_{ij}^F + J_{ij}^{AF}$.

Using the model of localized orbitals developed by Kahn et al.,[21d] J_{ij}^F can be expressed as $J_{ij}^F = 2k_{ij}$, in terms of the bielectronic exchange integral

$$k_{ij} = \langle a_i(1) b_j(2) | 1/r_{12} |\ a_i(2) b_j(1) \rangle$$

while J_{ij}^{AF} can be written as $J_{ij}^{AF} = t_{ij}\hat{e}S_{ij}$, where t_{ij} is the transfer integral and S_{ij} is the overlap between the orbitals a_i and b_j: Sij = $\langle a_i(1)|b_j(1)\rangle$.

At first order, t_{ij} is proportional to S_{ij} so that J_{ij}^{AF} is proportional to S_{ij}^2; i.e., the stronger the overlap, the stronger the antiferromagnetic contribution. Orbitals orthogonal by symmetry (strictly orthogonal) will have $S_{ij} = 0$ and will not contribute to the antiferromagnetism. Usually, the antiferromagnetic contributions are much larger than the ferromagnetic

(19) (a) Matsumoto, N.; Ōkawa, H.; Kida, S.; Ogawa, T.; Ohyoshi, A. *Bull. Chem. Soc. Jpn.* 1989, *62*, 3812. (b) Sato, Y.; Miyasaka, H.; Matsumoto, N.; Ōkawa, H. *Inorg. Chim. Acta*, in press.

(20) Schwartz, M.; Hatfield, W. E.; Joesten, M. D.; Hanack, M.; Datz, A. *Inorg. Chem.* **1985**, *24*, 4198.

(21) (a) Anderson, P. W. In *Magnetism*; Rado, G. T., Suhl, H., Eds.; Academic: New York, 1963; Vol. 1, p 25. (b) Goodenough, J. B. *Magnetism and the Chemical Bond*; Wiley: New York, 1963. (c) Hay, P. J.; Thiebault, J. C.; Hoffmann, R. *J. Am. Chem. Soc.* **1975**, *97*, 4884. (d) Reference 18b, p 37.

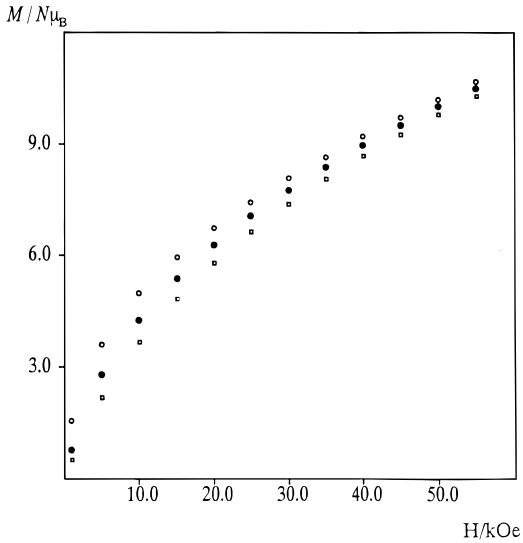

Figure 18. Magnetization as a function of the applied magnetic field for **9**, performed at 1.9 K (○), 4.5 K (□), and 6.0 K (●).

ones, so that only one antiferromagnetic path (i.e., a couple *i*,*j* for which $S_{ij} \neq 0$) is often sufficient to lead to an overall antiferromagnetic coupling, $J < 0$, between the two centers. If, however, all the orbitals are orthogonal, the overall interaction will be ferromagnetic, $J > 0$.

These concepts have been widely employed in the interpretation of the nature of the magnetic interactions through CN^- bridges in the Prussian blue family.[12a,13,22] For example, a combination of Ni(II)−Cr(III) gives an ideal system for showing ferromagnetic interaction because three unpaired electrons of Cr(III) occupy the $(t_{2g})^3$ configuration and the two unpaired electrons of Ni(II) occupy the $(e_g)^2$ configuration, so that the six J_{ij} contributions are all ferromagnetic due to the strict orthogonality.

For the compounds reported in this study we have observed trimeric and pentameric units made from CN-bridged Fe(III) and Mn(III) species, which show small ferromagnetic Mn(III)−Fe(III) interactions. A smaller ferromagnetic coupling has been observed also for intertrimer CN-bridged Mn(III)−Fe(III) interactions which make up the bidimensional structure in compound **6**.

An analysis of the Mn(III)−Fe(III) system (high-spin d^4, $(t_{2g})^3(e_g)^1$, low-spin d^5, $(t_{2g})^5$) similar to that of the Prussian blue family leads to the conclusion that both ferromagnetic and antiferromagnetic contributions coexist and that an overall antiferromagnetic coupling would be expected.

We must, however, take into account that the Prussian blue family shows highly symmetric cubic structures in which the M−C−N−M units are perfectly colinear and the metals have regular octahedral coordination. In our case the geometry of the M-C-N-M units is less regular, with one of the metals, Mn, in a six coordinate bipyramidal coordination and the C-N-Mn angle different from 180°, at least for the pentamer and the intertrimer interactions. We also recall that an unexpected antiferromagnetic coupling has been observed between two CN^- bridged bipyramidal Cr(III) [d^3, $(t_{2g})^3$], in the *catena*-cyano(phthalocyaninato)chromium(III).[20]

We have considered possible orbital explanations for the observed intertrimer ferromagnetic coupling. In order to discuss the orbital interactions in the trimeric units, we have set the Mn−Fe−Mn bond along the *z*-axis, with the origin on Fe and pointing the *x*- and *y*-axes toward the equatorial CN^- groups.

(22) Klenze, R.; Kanellakopulos, B.; Trageser, G.; Eysel, H. H. *J. Chem. Phys.* **1980**, *72*, 5819.

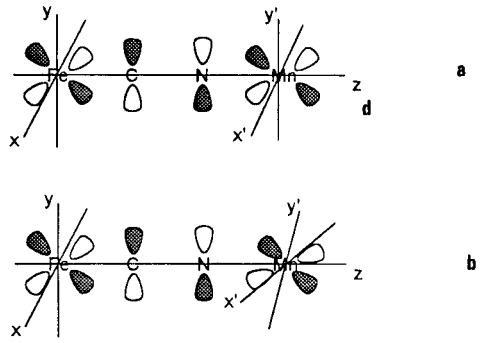

Figure 19. Schematic orbital interaction in the $(CN)_6Fe-CN-Mn$-(BS) unit between d_{xy}(Fe) and d_{xz}(Mn): (a) parallel *xy* local axis on Fe and Mn, (b) local axis rotated 45°.

As far as the local axis on Mn is concerned, *z* is the same while *x* and *y* point toward the two N atoms and the two O atoms of the quadridentate Schiff base ligand. First consider the Mn-(III) situation: the $d_{x^2-y^2}$ is far higher in energy, so that the four unpaired electrons are in the d_{xy}, d_{xz}, d_{yz} and d_{z^2} orbitals. In the Fe(III) ion, with a pseudooctahedral configuration, the five electrons occupy the three t_{2g} electrons, leaving only one unpaired.

Considering, at first order, the configuration around Fe(III) as perfectly octahedral, the electronic configurations with the unpaired electron on d_{xy}, d_{xz}, or d_{yz} are degenerate, and therefore equally populated with a statistical factor of 1/3. If the *x* and *y* local axes on Mn(III) were parallel to the *x* and *y* local axes on Fe(III), as usually happens in compounds of the Prussian blue family, there would be two antiferromagnetic paths corresponding to the d_{xz}(Mn)−d_{xz}(Fe) and d_{yz}(Mn)−d_{yz}(Fe) nonzero overlaps.

However, these two couples of local axes are rotated by approximately 45° with respect to the common *z* axis and almost bisect each other. As a consequence, the d_{xz}(Mn) and d_{xz}(Fe) orbitals, as well as the d_{yz}(Mn) and d_{yz}(Fe) ones, do not point toward each other and the overlap is strongly reduced (see Figure 19).

The large number of ferromagnetic paths could therefore overcome these two reduced antiferromagnetic contributions giving an overall, small, ferromagnetic interaction. The same explanation applies to the intertrimer interaction observed in compound **6**. Here the interaction is smaller because of the longer N−Mn distance.

This explanation cannot be applied to the pentamer unit where the local axes are rotated. However, in this case, the C−N−Mn angle is 156°, and this bending should reduce the overlap between the magnetic orbitals and weaken the antiferromagnetic paths.

Concluding Remarks

Extended Mn(III)−Fe(III) structures have been obtained from the reaction of $[Mn(BS)(H_2O)]^+$ cations and the $[Fe(CN)_6]^{3-}$anion. The assembly mode of the two components is achieved thanks to the bonding mode of the bridging CN^- anion and is largely dictated by the steric properties of the Schiff base ligand around manganese. These are mainly responsible for the occurrence of the cation in a monomeric or dimeric form. In the former case we produce the 2:1 structures shown in complexes **6**, **7**, and **8**, where the building block is the $[\{Mn(BS)\}_2\{Fe(CN)_6\}]^-$ trimer. In the latter case we produce the 4:1 structure **9** which contains the pentanuclear building block $[\{Mn(saltmen)\}_4\{Fe(CN)_6\}]^+$. The assembly mode assured by cations and anions on the above-mentioned building blocks gives rise to three-dimensional structures. Depending on such an assembly mode,

we discovered materials having significantly different magnetic behavior. While **7** and **8** assume a discrete trimeric structure, **6** has an extended two-dimensional layer structure consisting of a cyclic octamer $[(-Mn-NC-Fe-CN-)]_4$ as a net unit and shows a metamagnetic behavior with a Neel temperature T_N = 9.2 K and a critical field at 2 K of 300 Oe, where the ferromagnetic interaction operates within each layer and the antiferromagnetic interaction operates between the layers. **9** has a two-dimensional layer structure consisting of dodecamer $[(\text{-NC-Fe-CN-Mn}\cdots\text{Mn-})]_4$ as a repeating unit and shows a ferromagnetic behavior with the a Curie temperature T_c = 4.5 K, where two kinds of intralayer magnetic interaction are both ferromagnetic (interaction between Fe(III) and Mn(III) through CN and that between Mn(III) and Mn(III)) in the out-of-plane dimeric unit) and interlayer interaction is also weakly ferromagnetic. The above amazing versatility in the chemical formulation, crystal structure, and magnetism can be brought on by the properties of the manganese(III) Schiff base complex. We are now working on a novel family of extended multidimensional compounds by use of the manganese(III) Schiff base component and the other building component.[23]

Experimental Section

General Procedure. All chemicals and solvents used for synthesis were reagent grade. The quadridentate Schiff base ligands H_2L (H_2-5-Clsalen, H_2-5-Brsalen, H_2-3-MeOsalen, H_2salen, H_2saltmen, and H_2-salcy) were synthesized by mixing the corresponding salicylaldehyde and the diamine in a 2:1 mole ratio in methanol according to the literature.[24] $K_3[Fe(CN)_6]$ was purchased from Wako Pure Chemical Industries Ltd. and used without further purification. Since $K_3[Fe(CN)_6]$ has a tendency to decompose on heating and irradiation, the syntheses of the iron(III)−manganese(III) complexes were performed at room temperature and crystallization was performed in a dark room. **Caution:** Perchlorate salts are potentially explosive and should only be handled in small quantities.

Preparation of Manganese(III) Complexes $[MnL(H_2O)]ClO_4$ (H_2L = H_2-5-Clsalen, 1; H_2-5-Brsalen, 2; H_2-3-MeOsalen, 3; H_2saltmen, 4; and H_2salcy, 5). The manganese complexes were prepared by mixing manganese(III) acetate dihydrate, H_2L, and $NaClO_4$ in methanol in a molar ratio of 1:1:1.5 according to the method reported previously.[25] The complexes were obtained as dark brown crystals and identified by C, H, and N microanalyses and by the characteristic bands in their IR spectra.

Preparation of 6P. To a solution of **1** (0.294 g, 0.5 mmol) in 50 mL of methanol was added a solution of $K_3[Fe(CN)_6]$ (0.165 g, 0.5 mmol) in 5 mL of water at room temperature. The resulting solution was allowed to stand for 1 h, and the reddish brown precipitate thus produced was collected by suction filtration, washed with 1:1 (v/v) methanol−water and dried in vacuo to give a red-brown powder. Anal. Calcd for $C_{42}H_{36}N_{10}O_8KMn_2Fe$: C, 49.77;H, 3.58; N, 13.18; Mn, 10.84; Fe, 5.51. Found: C, 49.63; H, 3.68; N, 13.57; Mn, 10.63; Fe, 5.03. IR (KBr): ν(C≡N), 1601, 1624 cm^{-1}; ν(C≡N), 2097, 2114 cm^{-1} Mp >300 °C.

Preparation of 6C. Into a *N*,*N*-dimethylformamide solution of **1** (0.25 mmol in 30 mL DMF) was diffused a 2-propanol−water mixed solution of $K_3[Fe(CN)_6]$ (0.25 mmol in 30 mL of mixed solution). After standing for one week at room temperature in a dark room, brown, thin, plate crystals were obtained. The red-brown crystals thus obtained contain two *N*,*N*-dimethylformamide molecules per trinuclear unit as the crystallization solvent. d_m = 1.49 g cm^{-3} (measured by the flotation method in benzene−tetrachloromethane). IR (KBr): ν(C═N), 1601, 1625 cm^{-1}; ν(C≡N), 2100, 2114 cm^{-1}. Mp: >300 °C.

Preparation of 7. To a solution of **2** (0.254 g, 0.5 mmol) in 50 mL of methanol was added a solution of $K_3[Fe(CN)_6]$ (0.165 g, 0.5 mmol) in 5 mL of water at room temperature. The resulting solution was allowed to stand for 1 h, and the yellow-brown precipitate thus obtained was collected by suction filtration, washed with 1:1 (v/v) methanol−water, and dried in vacuo to give a pale, yellow-brown powder. Anal. Calcd for $C_{32}H_{32}N_{10}O_8Cl_4FeKMn_2$: C, 41.37; H, 2.92; N, 12.70; Mn, 9.96; Fe, 5.06. Found: C, 41.42; H, 2.95; N, 12.46; Mn, 10.17; Fe, 4.83. IR (KBr): ν(C═N), 1600−1636 cm^{-1}; ν(C≡N), 2104, 2114, 2129 cm^{-1}. Mp: >300 °C.

Preparation of 8. To a solution of **3** (0.298 g, 0.5 mmol) in 50 mL of methanol was added a solution of $K_3[Fe(CN)_6]$ (0.165 g, 0.5 mmol) in 5 mL of water at room temperature. The resulting solution was allowed to stand for 1 h, and the green-brown precipitate thus produced was collected by suction filtration, washed with 1:1 (v/v) methanol−water, and dried in vacuo to give a green-brown powder. Anal. Calcd for $C_{32}H_{32}N_{10}O_8Br_4FeKMn_2$: C, 35.63;H, 2.52; N, 10.93; Mn, 8.58; Fe, 4.36. Found: C, 35.99; H, 2.57; N, 10.64; Mn, 8.69; Fe, 3.91. IR (KBr): ν(C═N), 1635 cm^{-1}; ν(C≡N), 2104, 2112, 2127 cm^{-1}. Mp: >300 °C.

Preparation of 9P. To a solution of **4** (0.247 g, 0.5 mmol) in 50 cm^3 of methanol was added a solution of $K_3[Fe(CN)]_6$ (0.165 g, 0.5 mmol) in 5 cm^3 of water at room temperature. The resulting solution was allowed to stand for 1 h, and the brown precipitate thus produced was collected by suction filtration, washed with 1:1 (v/v) methanol−water, and dried in vacuo to give a red-brown powder. Anal. Calcd for $C_{86}H_{94}N_{14}O_{15}ClFeMn_4$: C, 55.10;H, 5.05; N, 10.46; Mn, 11.72; Fe, 2.98. Found: C, 54.90; H, 4.76; N, 10.39; Mn, 11.74; Fe, 2.94. IR (KBr): ν(C═N), 1600−1630 cm^{-1}; ν(C≡N), 2118 cm^{-1}; ν(Cl−O), 1096−1144 cm^{-1}. Mp: >300 °C.

Preparation of 9C. Crystals suitable for single-crystal X-ray analysis were prepared by the same diffusion method as that used in the preparation of **6C**. The methanol solution of **4** (0.25 mmol in 30 cm^3 of methanol) and an aqueous solution of $K_3[Fe(CN)]_6$ (0.25 mmol in 30 cm^3 of water) were diffused slowly into each other using an H-type glass tube at room temperature. After standing for one week at room temperature in a dark room, well-defined dark brown, rhombic crystals were obtained. The crystals easily effloresce in the air to give a black-brown powder. d_m = 1.42 g cm^{-3} (flotation method in benzene−tetrachloromethane). IR (KBr): ν(C═N), 1600−1630 cm^{-1}; ν(C≡N), 2120 cm^{-1}; ν(Cl−O), 1100−1150 cm^{-1}. Mp: >300 °C.

Preparation of 10. To a solution of **5** (0.253 g, 0.5 mmol) in 50 cm^3 of methanol was added a solution of $K_3[Fe(CN)]_6$ (0.165 g, 0.5 mmol) in 5 cm^3 of water at room temperature. The resulting solution was allowed to stand for one week at room temperature in a dark room, and the black rhombic crystals thus produced were collected by suction filtration, washed with 1:1 (v/v) methanol−water, and dried in vacuo to give a yellow-brown powder. Anal. Calcd for $C_{86}H_{82}N_{14}O_{13}ClFeMn_4$: C, 56.42; H, 4.52; N, 10.71; Mn, 12.00; Fe, 3.05. Found; C, 56.43; H, 4.48; N, 10.67; Mn, 11.86; Fe, 2.83. IR(KBr): ν(C═N), 1600−1630 cm^{-1}; ν(C≡N), 2112 cm^{-1}; ν(Cl−O), 1096−1151 cm^{-1}. Mp: >300 °C.

Physical Measurements. Elemental analyses for C, H, and N were performed at the Elemental Analysis Service Center of Kyushu University. Manganese and Iron analyses were made on a Shimadzu AA-680 atomic absorption/flame emission spectrophotometer. Infrared spectra were measured on KBr disks with JASCO IR-810 and Shimadzu FTIR-8600 spectrophotometers. Densities were measured by the flotation method in mixed solutions of benzene and tetrachloromethane. Magnetic susceptibilities were preliminarily measured with a Faraday balance in the temperature range of 80−300 K and with a HOXSAN HSM-D SQUID magnetic susceptometer under the applied magnetic field of 100 G in the 4.2−100 K temperature range at Kyushu University, where the calibrations were made with $[Ni(en)_3]S_2O_3$ (en = ethylenediamine) for the Faraday balance and with $Mn(NH_4)_2(SO_4)_2 \cdot 6H_2O$ for the SQUID susceptometer.[26] Magnetic susceptibilities were

(23) Recently we have prepared the 1:1 compound with the formula of $(Et_4N)_2[Mn(acen)][Fe(CN)_6]$, where Et_4N = tetraethylammonium ion and acen = *N*,*N*′-ethylenebis(acetylacetonylideneiminato) dianion. The crystal structure analysis revealed that the compound assumes a linear one-dimensional structure. Unpublished result.

(24) Pfeifer, P.; Hesse, T.; Pfitzner, H.; Scholl, W.; Thielert, H. *J. Pract. Chem.* **1937**, *149*, 217.

(25) Matsumoto, N.; Takemoto, N.; Ohyoshi, A.; Ōkawa, H. *Bull. Chem. Soc. Jpn.* **1988**, *61*, 2984.

(26) Lindoy, L. F.; Katovic, V.; Busch, D. H. *J. Chem. Educ.* **1972**, *49*, 117.

Table 3. Experimental Data for the X-ray Diffraction Studies on Crystalline Compounds **6C** and **9C**

	6C	**9C**
chemical formula	$C_{48}H_{50}KFeMn_2N_{12}O_{10}$	$C_{86}H_{90}ClFeMn_4N_{14}O_{13}$
a (Å)	13.750(4)	18.756(3)
b (Å)	12.456(2)	18.756(3)
c (Å)	15.646(2)	28.279(5)
α (deg)	90	90
β (deg)	102.91(1)	90
γ (deg)	90	90
V (Å^3)	2612.1(9)	9948(1)
Z	2	4
fw	1159.82	1838.79
space group	$P2_1/c$	$I4/m$
λ (Å)	0.710 69	0.710 69
ρ_{calcd} (g cm^{-3})	1.475	1.228
μ (cm^{-1})	8.97	7.24
no. of reflections	3221	4488
R[a]	4.9	7.3
R_w[b,c]	5.0	11.3

[a] $R = \Sigma||F_o| - |F_c||/\Sigma|F_o|$. [b] $R_w = \{\Sigma[w(|F_o| - |F_c|)^2]/\Sigma[w|F_o|^2]\}^{1/2}$. [c] $w = 1/\sigma(F_o)^2$. Flotation method in benzene/tetrachloromethane.

measured at Lausanne University using a MPMS5 SQUID susceptometer (Quantum Design Inc.), where the applied magnetic fields were 600−800 G. Field dependences of magnetization up to 5.5 T, magnetic hysteresis loops, field-cooled magnetization, and remnant magnetization measurements were made on a MPMS5 SQUID susceptometer (Quantum Design Inc.). Corrections were applied for diamagnetism calculated from Pascal's constants.[27] Effective magnetic moments were calculated by the equation $\mu_{eff} = 2.828(\chi_M T)^{1/2}$, where χ_M is the magnetic susceptibility per formula unit. Fitting the magnetic data to the theoretical expression was performed by minimizing the agreement factor, defined as $F = \Sigma_i(\chi_i^{obsd} - \chi_i^{calcd})^2/\chi_i^{obsd}$ through a Levenberg−Marquart routine.

X-ray Data Collection and Reduction. Single crystals of **6C** and **9C** were prepared by the diffusion method described in the synthetic procedure. A single crystal of **6C** was cut from a thin plate crystal, mounted on a glass fiber, and coated with epoxy. Crystal dimensions were 0.5 × 0.3 × 0.1 mm for **6C**. As crystals of **9C** eliminate their crystallization solvents on decomposition, they were encapsulated in a glass capillary with a small amount of mother liquid, and the dimensions of the crystals were 0.2 × 0.15 × 0.3 mm. All measurements were made on a Rigaku AFC7R diffractometer with graphite monochromated Mo Kα radiation (λ = 0.710 69 Å) and a 12 kW rotating anode generator. The data were collected at a temperature of 20 ± 1 °C using the ω-2θ scan technique to a maximum 2θ value of 50.0° at a scan speed of 16.0 °deg/min (in ω). The weak reflections($I < 10.0\sigma(I)$) were rescanned (maximum of four scans), and the counts were accumulated to ensure good counting statistics. Stationary background counts were recorded on each side of the reflection. The ratio of peak counting time to background counting time was 2:1. The diameter of the incident beam collimator was 1.0 mm, the crystal to detector distance was 235 mm, and the computer-controlled detector aperture was set to 9.0 × 13.0 mm (horizontal vertical). The intensities of three representative reflections were measured after every 150 reflections. Over the course of the data collection, the standard reflections were monitored and the decay corrections were applied by a polynomial correction. An empirical absorption correction based on azimuthal scans of several reflections was applied. The data were corrected for Lorentz and polarization effects.

Solution and Refinement of Crystal Structures. The structures were solved by direct methods[28] and expanded using Fourier techniques.[29] The non-hydrogen atoms were refined anisotropically. Hydrogen atoms were included. Full matrix least-squares refinement based on observed reflections (**6C** had $I > 3.00\sigma(I)$ and **9C** had $I > 4.00\sigma(I)$) were employed, where the unweighted and weighted agreement factors of $R = \Sigma||F_o| - |F_c||/\Sigma|F_o|$ and $R_w = [\Sigma w(|F_o| - |F_c|)^2/\Sigma w|F_o|^2]^{1/2}$ were used. The weighting scheme was based on counting statistics. Plots of $\Sigma w(|F_o| - |F_c|)^2$ versus $|F_o|$, the reflection order in the data collection, sin θ/λ, and various classes of indices showed no unusual trends. Crystal data and details of the structure determinations are summarized in Table 3.

Neutral atomic scattering factors were taken from Cromer and Waber.[30] Anomalous dispersion effects were included in F_{calcd}; the values $\Delta f'$ and $\Delta f''$ were those of Creagh and McAuley.[31] The values for the mass attenuation coefficients are those of Creagh and Hubbel.[32] All calculations were performed using the teXsan crystallographic software package of the Molecular Structure Corp.[33] In complex **9C**, the fragility of the crystals made it difficult to improve the quality of the X-ray analysis and because of high symmetry in the crystal group $I4/m$ and the existence of disordering, the atoms which constitute the perchlorate ion were refined isotropically.

Acknowledgment. This work was supported by the Tokuyama Science Foundation and Ministry of Education, Science, and Culture of Japan (Grant-in-Aid for Scientific Research (No. 04453048)), the Fonds National Suisse de la Recherche Scientifique (Grant No. 20-40268.94), and the Fondation Herbette, University of Lausanne (N.R.).

Supporting Information Available: Figures S1, S2, and S3 showing an ORTEP drawing, projections along and perpendicular to the *b* axis, and a space-filling representation of the three-dimensional packing structure for {[Mn(salen)]$_3$[Fe(CN)$_6$]·3MeOH·5H$_2$O} and text describing data collection and reduction and structure solution and refinement and tables giving crystallographic data, fractional atomic coordinates, anisotropic displacement parameters, complete lists of bond distances and angles, and thermal parameters for **6**, **9**, and {[Mn(salen)]$_3$[Fe(CN)$_6$]·3MeOH·5H$_2$O} (68 pages). This material is contained in many libraries on microfiche, immediately follows this article in the microfilm version of the journal, can be ordered from the ACS, and can be downloaded from the Internet; see any current masthead page for ordering information and Internet access instructions.

JA952706C

(27) Boudreaux, E. A.; Mulay, L. N. *Theory and Applications of Molecular Paramagnetism*, John Wiley and Sons: New York, 1976; pp 491−495.

(28) SAPI91: Fan Hai-Fu. Structure Analysis Programs with Intelligent Control, Rigaku Corp., Tokyo, Japan, 1991. MULTAN88: Debaerdemaeker, T.; Germain, G.; Main, P.; Refaat, L. S.; Tate, C.; Woolfson, M. M. Computer program for the automatic solution of crystal structures from X-ray diffraction data, University of York, U.K., 1988. SHELXS86: Sheldrick, G. M. A program for X-ray crystal structure determination, University of Cambridge, 1986.

(29) DIRDIF92: Beurskens, P. T.; Admiraal, G.; Beurskens, G.; Bosman, W. P.; Garcia-Granda, S.; Gould, R. O.; Smits, J. M. M.; Smykalla, C. The DIRDIF program system. Technical Report of the Crystallography Laboratory; University of Nijmegen: The Netherlands, 1992.

(30) Cromer, D. T.; Waber, J. T. *International Tables for X-ray Crystallography*; The Kynoch Press: Birmingham, England, 1974; Vol. IV, Table 2.2A.

(31) Creagh, D. C.; McAuley, W. J. In *International Tables for Crystallography*; Wilson, A. J. C., Ed., Kluwer Academic Publishers: Boston, 1992; Vol. C, pp 219−222, Table 4.2.6.8.

(32) Creagh, D. C.; Hubbel, J. H. In *International Tables for Crystallography*; Wilson, A. J. C., Ed.; Kluwer Academic Publishers: Boston, 1992; Vol. C, pp 200−206, Table 4.2.4.3.

(33) teXsan: Crystal Structure Analysis Package, Molecular Structure Corp. 1985, 1992.